Monoallelic *KCNB2* variants lead to a neurodevelopmental disorder caused by altered channel inactivation.

Shreyas Bhat,[1] Justine Rousseau,[2] Coralie Michaud,[2] Charles Marques Lourenço,[3] Joan M Stoler,[4] Raymond J Louie,[5] Lola K Clarkson,[5] Angie Lichty,[5] Daniel C Koboldt,[6] Shalini C Reshmi,[7] Sanjay M Sisodiya,[8] E.M.M. Hoytema van Konijnenburg,[9] Klaas Koop,[9] Peter M van Hasselt,[10] Florence Démurger,[11] Christèle Dubourg,[12] Bonnie R Sullivan,[13] Susan S Hughes,[13] Isabelle Thiffault,[14] Elisabeth Simard Tremblay,[15] Andrea Accogli,[16] Myriam Srour, [17] Rikard Blunck,[1] and Philippe M Campeau[18]

Affiliations:

1 Center for Interdisciplinary Research on Brain and Learning (CIRCA), Department of Physics and Department of Pharmacology and Physiology, Université de Montréal, Montréal, QC, Canada

2 Centre de Recherche du Centre Hospitalier Universitaire Sainte-Justine, Université de Montréal, Montréal, QC, Canada, H3T 1C5

3 Charles Marques Lourenço : Centro Universitário Estácio de Ribeirão Preto, São Paulo, Brazil.

4 Division of Genetics and Genomics, Boston Children's Hospital, Boston, MA, USA.

5 Greenwood Genetic Center, Greenwood, SC, 29646, USA

6 Steve and Cindy Rasmussen Institute for Genomic Medicine at Nationwide Children's Hospital , Columbus, OH, USA.

19 7 Department of Pathology and Laboratory Medicine, Nationwide Children's Hospital, Columbus,
20 OH, USA.

21 8 Department of Clinical and Experimental Epilepsy, University College London Queen Square
22 Institute of Neurology, London, WC1N 3BG UK.

23 9 Department of Metabolic Diseases, Wilhelmina Children's Hospital, University Medical Center
24 Utrecht, Utrecht the Netherlands.

25 10 Department of Genetics, Section Metabolic Diagnostics, University Medical Center Utrecht,
26 Utrecht, the Netherlands.

27 11 Service de Génétique, CHBA, Vannes 56000, France.

28 12 Department of Molecular Genetics and Genomics, Rennes University Hospital, Rennes, France;
29 Univ Rennes, CNRS, IGDR, UMR 6290, Rennes, France.

30 13 Division of Clinical Genetics, Department of Pediatrics, Children's Mercy Kansas City, Kansas
31 City, MO, USA.

32 14 Departments of Pediatrics and of Pathology and Laboratory Medicine, Children's Mercy Kansas
33 City, Kansas City, MO, USA.

34 15 Department of Neurology and Neurosurgery, McGill University Health Centre, Montréal, QC,
35 Canada.

36 16 Research Institute of the McGill University Health Centre, Montréal, QC, Canada.

17 Department of Pediatrics, Division of Pediatric Neurology, McGill University, Montréal, QC, Canada.

18 Department of Pediatrics, Université de Montréal, Montréal, QC, Canada.

Correspondence emails:

Rikard Blunck

Address: Department of Physics and Department of Pharmacology and Physiology, Université de Montréal, Montréal, QC, Canada2960 Chemin de la Tour, Montréal, QC H3T 1J4, Canada.

Email: rikard.blunck@umontreal.ca

Philippe M. Campeau

Address: Department of Pediatrics, CHU Sainte Justine Research Center, University of Montreal, Côte-Sainte-Catherine, Montreal, QC H3T 1C5, Canada.

Email: p.campeau@umontreal.ca

Running title: Pathogenic KCNB2 variants affect K^+ channel activation and inactivation.

Keywords: Dysmorphism, global developmental delay, epilepsy, KCNB2, channel inactivation

Abbreviations: Kv: voltage gated potassium channels, AP: action potential, cRNA: complementary RNA, GV: conductance-voltage, IV: current-voltage, Inac-V: Inactivation-voltage, POPC: 1-palmitoyl-2-oleoyl-sn-glycero-3-phosphocholine, POPE: 1-palmitoyl-2-oleoyl-sn-glycero-3-phosphoethanolamine, DPSM: stearoyl-sphingomyelin, POPS: 1-palmitoyl-2-oleoyl-sn-glycero-3-phospho-L-serine, POPI: 1-palmitoyl-2-oleoyl-sn-glycero-3-phosphoinositol, WT – wild type.

Abstract

Ion channels mediate voltage fluxes or action potentials that are central to the functioning of excitable cells such as neurons. The *KCNB* family of voltage-gated potassium channels (Kv) consists of two members (*KCNB1* and *KCNB2* genes) that encode KCNB1 and KCNB2 channels, respectively. These channels are major contributors to delayed rectifier potassium currents arising from the neuronal soma which modulate overall excitability of neurons. In this study, we identified several monoallelic pathogenic missense variants in the *KCNB2* gene, in individuals with neurodevelopmental disorders and other neurological conditions such as epilepsy and autism. Recurrent dysmorphisms included a broad forehead, synophrys and digital anomalies. Additionally, we selected three variants where genetic transmission has not been assessed, from two epilepsy studies. We characterized channel properties of these variants by expressing them in oocytes of *Xenopus laevis* and conducting cut-open oocyte voltage clamp electrophysiology. Our datasets indicate no significant change in absolute conductance and conductance-voltage relationships of most disease variants as compared to wild type (WT), when expressed either alone or co-expressed with WT-KCNB2 (except for c.1141A>G, (p.Thr381Ala) and c.641C>T, (p.Thr214Met), which show complete abrogation of currents when expressed alone with the former exhibiting a left shift in activation midpoint when expressed alone or with WT-KCNB2). These variants, however, show collective features of increased inactivation shifted to hyperpolarized potentials. We suggest that the effects of the variants on channel inactivation may contribute to hyper-excitability of neurons, which leads to disease onset.

Introduction

The *shab*-related *KCNB* sub-family of voltage-gated potassium (Kv) channels consists of two genes *KCNB1* [MIM 600397] and *KCNB2* [MIM 608164] that encode KCNB1 (Kv2.1) and KCNB2 (Kv2.2) channels, respectively[1]. KCNB1 is well documented as being ubiquitously expressed in several brain regions[2]. Characterization of KCNB2 expression in the brain, in comparison, is less defined due to discrepancies in KCNB2 cloning, and concurrent antibodies used in different studies[3]. Early studies professed mutual exclusivity of subcellular distribution of KCNB1 and KCNB2 in both principal and inhibitory neurons co-expressing them and by extension their roles in controlling neuronal excitability; KCNB1 is restricted to large clusters in the proximal dendrites and soma of neurons[4,5], while KCNB2 is diffusely localized in neuronal dendrites[6-8]. However, recent reports have detailed KCNB2 expression to localise similarly to KCNB1 in cortical neurons although other neurons may express high levels of KCNB1 or KCNB2 but not both[3,9,10]. In addition to the cortical expression in the central nervous system, KCNB2 has also been identified in the medial nucleus of the trapezoid body[11], the basal forebrain[12,13] and the spinal cord[14]. Single-cell RNAseq data show a high expression in excitatory neurons as well as various types of interneurons (Allen Brain Map, Human MTG 10x SEA-AD dataset).

KCNB1 and KCNB2, like other Kvs, are outward rectifiers, i.e., they conduct K^+ from the cytosol to the extracellular space and provide repolarizing currents that return a depolarized neuron back to the resting state. These channels activate and inactivate slowly compared to the depolarizing sodium currents. Activation is achieved at suprathreshold voltage during an action potential (AP). Such slow activation and inactivation kinetics prolong the duration of KCNB-mediated K^+ conductance; these properties are instrumental to their regulation of repolarization and

hyperpolarization phases of an action potential[15,16]. Consequently, KCNBs help determine interspike interval, AP amplitude and AP firing fidelity during high frequency firing[11,17-20]. Assigning these effects to neuronal excitability on homotetrameric complexes of either KCNB1 or KCNB2 is a simplified view. KCNB1 and KCNB2 have been shown to form heterotetrameric complexes both *in vitro* and *in vivo*[3,9] . In addition, KCNB channels co-assemble with the electrically silent KvS channels and auxiliary β-subunits to form heterotetrameric protein complexes that display drastically different biophysical and pharmacological properties as compared to their homotetetrameric counterparts[21,22]. In addition to their role in mediating K^+ conductance, KCNB1 and KCNB2 also exist as non-conducting clusters caused by the formation of ER/plasma membrane junctions that have numerous functions such as inter-organelle communication and calcium signalling, to name a few[2].

Over 29 distinct pathogenic variants in *KCNB1* gene that either truncate or alter the protein sequence of the KCNB1 channels have been identified in individuals suffering from early onset developmental and epileptic encephalopathies [MIM 616056] [23,24]. The *KCNB1* variants that were functionally characterized were shown in non-native systems to exhibit a multitude of effects on channel activity such as abolished channel function, reduced current density, deficits in voltage sensing, loss in ion selectivity and gain of inward cation conductance[24-27]. Expression of some of these variants in cortical neurons led to reduced repetitive firing properties[26]. Of note, *KCNB1* KO (*KCNB1*$^{-/-}$) mice have preserved brain anatomy, and do not exhibit spontaneous epileptic seizures, or visual or motor impairment[28]. Hippocampal slices of these mice, however, exhibit drug-induced hyperexcitability and stimulation-induced epileptiform activity. Interestingly, homozygous mice expressing a *KCNB1* variant (p.G379R) developed spontaneous seizures as well as proconvulsant-

and handling-induced seizures along with being hyperactive, impulsive and having reduced anxiety[29].

In this study, we identified several variants in the *KCNB2* gene in individuals with neurodevelopmental disorders that has not been associated with a Mendelian genetic disorder in humans in OMIM previously. Most exhibited developmental delays while some also had epilepsy, ADHD, and autism. In addition, we screened the Epi25K dataset and another epilepsy cohort and identified three additional candidate variants. We performed electrophysiological characterization of these variants in oocytes from *Xenopus laevis*. Our data suggests that most *KCNB2* variants show common features of increased channel inactivation with the voltage dependence shifted to hyperpolarized potentials. Based on these observations, we hypothesize that the effects of the variants on channel inactivation may contribute to reduced KCNB2 availability, leading to hyper-excitability of neurons and to disease onset.

Materials and Methods

Clinical and genetic investigations

Variants were identified by trio sequencing of probands. Exome sequencing methods have been described elsewhere (see following references for individuals 1[30], 2[31], 3[32], 4[33], 5[34], 6[35] and 7[36]. The cohort was assembled with the help of Matchmaker Exchange platform tools[37]. All clinical information is shared in accordance with local institutional ethical review boards and is in accordance with the ethical standards of the responsible committee on human experimentation (institutional and national) and proper informed consent. A consent for the publication of the photographs included here was obtained from parents or legal guardians.

Molecular Biology and Channel Expression.

Oocytes from *Xenopus laevis* were surgically obtained as described elsewhere[38]. The human KCNB2 (NM_004770.3) cDNA in pcDNA3.1(+) N-terminus HA tag was purchase at Genescript (Clone ID: OHu25595C). All variants were introduced in KCNB2 construct using the QuikChange Lightning site-directed mutagenesis kit (Agilent Technologies, USA) and were subcloned in pcDNA3.1 containing no tag using EcoR1/XhoI restriction sites. The variants and primers (rev/fwd) are listed in Table S1. To generate high quality and high copy number plasmids, the plasmids were amplified using the CopyCutter EPI400 competent bacteria (Lucigen) to decrease insert toxicity and avoid non-desired additional mutations. cRNA was generated by linearizing the plasmids with a restriction enzyme (*DraIII*) and using the plasmid template for *in vitro* transcription using the mMESSAGE mMACHINE™ T7 ULTRA Transcription Kit (Thermo Fisher Scientific, U.S.A.). For functional expression of the KCNB2 channels, either 1 ng of WT

or individual mutant cRNA or 0.5 ng each of WT and one of the mutant cRNA was injected into oocytes and incubated for 12-24 h at 18°C to allow for channel expression.

Electrophysiology

Voltage clamping experiments were performed with a CA-1B amplifier (Dagan Corporation, U.S.A.). Currents were recorded in the cut-open oocyte voltage-clamp configuration[39]. The external solution used for ionic current recordings contained (in mM): 5 KOH, 110 N-methyl-D-glucamine (NMDG), 10 HEPES, and 2 $Ca(OH)_2$, pH adjusted to 7.1 with methanesulfonic acid (MES). The internal solution contained (in mM): 115 KOH, 10 HEPES, and 2 EDTA, pH adjusted to 7.1 with MES. The oocytes were placed in a three-part chamber (upper, middle and bottom) containing the external solution. Oocyte membrane exposed in the bottom chamber was permeabilized with 0.2% saponin in internal solution for 30s-1 min for direct current injection into the oocyte. Saponin was washed out and bottom chamber filled with internal solution. Conductance and inactivation of KCNB2 variants were recorded using the protocols illustrated in Fig. 3 and Fig. 5. Both conductance-voltage relation (GV) and Inactivation-voltage relation (Inac-V) was fit to a sum of two Boltzmann relation of the form G/Gmax = Minimum + (Amplitude1-Minimum)/(1 + exp((V50(1)-X)/k1)) + (Amplitude2-Amplitude1)/(1 + exp((V50(2)-X)/k2)) and I/Imax = Maximum + (Amplitude1-Maximum)/(1 + exp((V50(1)-X)/k1)) + (Amplitude2-Amplitude1)/(1 + exp((V50(2)-X)/k2)), respectively. The decision to use this fit was based on its fidelity and does not necessarily model the underlying processes. Reversal potential for KCNB2 variants were determined using the deactivation protocol illustrated in Fig.4. The external and internal solutions used for these recordings are described in Fig.4. The concomitant current-voltage relation was fit to a straight line (linear regression) between -90 and -50 mV; the x-intercept was

tabulated as the reversal potential. All data was acquired using the AnalysisX2 software (Département de physique, Université de Montréal, Canada) and analyzed and compiled using MatlabR2022a (The MathWorks, Inc., U.S.A.). Data shown are mean ± SD with $n \geq 5$ from at least two independent injections.

Molecular dynamics

We created an *in silico* homology model of full-length KCNB2 based on the known structure of the Kv1.2/2.1 chimera[40]. The model was generated using alphafold2[41]. The variants discussed here in the manuscript were introduced into the homology structure and the channels set into an *in silico* membrane containing: outer leaflet: POPC:POPE:DPSM in a molar ratio of 59:9:32 and inner leaflet: POPC:POPE:POPS:DPSM:POPI in a molar ratio of 25:38:16:14:7. The system was set in water containing 150mM KCl at a temperature of 300K using charmm-gui[42-44]. The different mutant channels as well as the wildtype channel were equilibrated and simulated *in silico* for 100 ns using NAMD[45].

Results

Clinical characteristics

The clinical phenotypes of the six individuals with *de novo* or dominantly transmitted variants in *KCNB2* are outlined in Table 1. Five variants were *de novo*, and one was inherited from a symptomatic father. Proband 7 inherited the variant from an unaffected mosaic father. The age at last evaluation ranged from 21 months of life to 18 years. Individuals were born at term and had normal birth growth parameters. Growth parameters, at last visit, were within the normal range in all individuals.

All seven individuals presented with global developmental delay. Six were diagnosed with intellectual disability. Three individuals presented with mild autistic traits while two were too young to make an autistic spectrum disorder (ASD) diagnosis. Two individuals were medicated with Levetiracetam for seizures. Two individuals had hypotonia including one with ataxic cerebral palsy. One individual was diagnosed with attention deficit/hyperactivity disorder (ADHD).

Five individuals presented with various facial dysmorphisms (Fig.1). Synophrys was observed in two individuals. A broad forehead was noted in two individuals. Hand anomalies were described in four individuals with one presenting with clinodactyly and another with nail hypoplasia. Mild blepharoptosis, beaked nose, flat mid face, frontal bossing, full lower lip, tongue protrusion and high palate were noted in one individual each.

Ophthalmological anomalies were found in four individuals. One individual presented with cortical vision impairment, Duane syndrome, hyperopia, astigmatism, and cataracts. Delayed visual maturation, myopia or severe strabismus were found in the other three individuals.

Two individuals had heart anomalies, notably one with aortic dilation and one with an abnormal trabeculation of the left ventricular myocardium. Two individuals had genitourinary malformations: one with a neurogenic bladder and the other with a suggestion of a slight shawl scrotum.

One individual was diagnosed with diabetes, gingival fibromatosis, low bone density, and oropharyngeal dysphagia. That individual (Proband 1 1, with the c.1141A>G, (p.Thr381Ala) variant) seemed to have more extensive involvement than the others (Supplemental Note: Case Reports), and her phenotype overlapped partially with Zimmerman-Laband (ZLS, [MIMs 135500, 616455, 618658]) and DOORS [MIM 220500] syndromes, which are neurodevelopmental disorders with epilepsy (treated with Levetiracetam) and hypoplasia of the terminal phalanges and nails. Of relevance, some of us have previously reported pathogenic variants in potassium channels KCNH1 [MIM 603305] and KCNN3 [MIM 602983] in ZLS [MIMs 135500, 618658][46,47], and vacuolar ATPase subunit ATP6V1B2 [MIM 606939] in ZLS [MIM 616455] and DOORS syndrome[46,48].

To identify additional candidate variants, we searched epilepsy study data. A missense variant (c.724G>A, (p.Ala242Thr)) was identified in an individual with Sudden Unexpected Death in Epilepsy (SUDEP), from a SUDEP study[49]. Additionally, c.472A>G, (p.Thr158Ala) was identified in two individuals with NAFE (non-acquired focal epilepsy, [MIM 604364, 245570]), and c.1124C>T, (p.Ala375Val) in one individual with GGE (genetic generalized epilepsy, [MIM

600669]), all from the Epi25 exome study variant server[50]. The variants were selected as they were absent in gnomAD and affected highly conserved residues. Additional clinical details or parental samples for segregation of the variants were not available to us, thus there is more uncertainty (compared to the 6 first variants identified) regarding the involvement of the variants in the neurological phenotypes of the individuals.

Using ACMG criteria[51] through the Varsome Classifier[52], all variants were predicted to be pathogenic or likely pathogenic (see criteria used in Table S2). The gnomAD missense tolerance score[53] for KCNB2 is relatively high with a Z score of 2.25 (range -5 to 5) since there were 511 expected missense variants but only 368 were observed. We have assessed the tolerance of each affected amino acid to missense variants using Metadome[54], and all amino acids are intolerant to missense variants, with scores in table S2 and the tolerance landscape of the proteins in figure S1. Additionally, table S2 shows the pathogenicity prediction and conservation scores obtained from Ensembl's Variant Effect Predictor for various commonly used tools[55].

Effect of *KCNB2* Variants on Functional Expression and Activation Kinetics

The topology of a KCNB2 monomer, like that of other Kv channels, consists of a N-terminus, hexahelical transmembrane domain including a pore-helix (P-loop ion selectivity filter) and a C-terminus (Fig. 2A). Most of the amino acids mutated in the *KCNB2* variants characterized in this study are highly conserved in homologous proteins across different species (Fig. 2B) and in human KCNB1 (not shown). The exception is amino acid position 646 (hKCNB2), which exists as alanine in some species (including humans) and co-incidentally as valine in others. 3D protein structures of KCNB2 and distribution of the variants characterised in this study are shown in tetrameric (top

view, Fig. 2C) and monomeric configuration (side view, Fig. 2D) based on the homology model of the known structure of the Kv1.2/2.1 chimera[40].

To assess biophysical properties and functional expression of the KCNB2 mutants, the cRNAs generated from the plasmids encoding the individual mutants were injected into oocytes of *Xenopus laevis* either alone (1 ng) or in equal amounts with WT-KCNB2 (0.5 ng each). 16-24 hours post-injection, the currents were studied using the cut-open oocyte voltage clamp technique. To record absolute amplitudes of K^+ conductance, the channels were held at -90 mV followed by a depolarising pulse to 100 mV for 200 ms (Fig. 3A). Most variants, when expressed either alone or with WT, did not show a significant change in current amplitudes when compared to WT. Exceptions are the c.641C>T, (p.Thr214Met) and c.1141A>G, (p.Thr381Ala) variants; these mutants showed complete and strong abrogation of K^+ conductance, respectively (Fig. 3B). K+ conductance was rescued when the mutants were co-expressed with WT-KCNB2 (Fig. 3D). The c.641C>T, (p.Thr214Met) variant, when co-expressed with WT-KCNB2, and the c.994T>G, (p.Tyr332Asp) variant, when expressed alone, show significant reduction in current amplitudes as compared to WT-KCNB2 (Fig. 3B and 3D, Table 2).

We next characterised the activation properties of the *KCNB2* variants by analyzing their conductance-voltage (GV) relationship. Conductance can be inferred from the tabulation of the isochronal current amplitudes at the beginning of the -20 mV step in Fig. 3A. The representative raw traces of the corresponding currents are presented from an oocyte that either expresses the individual variants alone (top) or co-expresses both the individual variant and WT (below). The c.641C>T, (p.Thr214Met)variant was excluded from the GV analyses due to lack of any activation currents by this mutant. The GV datasets (Fig. 3C and 3E) were best fitted by a sum of two

Boltzmann distribution that generated two activation midpoints ($V_{50(1)}$ and $V_{50(2)}$) and two corresponding slope factors (k_1 and k_2, respectively). These parameters are compiled in Table 2. Of all variants, GV profiles of c.1141A>G, (p.Thr381Ala) and c.994T>G, (p.Tyr332Asp) channels showed significant differences when compared to those of WT. However, while c.1141A>G, (p.Thr381Ala) channels showed a $\sim$20 mV shift to hyperpolarized potentials in activation $V_{50(1)}$ compared to WT, c.994T>G, (p.Tyr332Asp) was shifted by 5 mV to depolarized potentials. The other mutants did not show significant differences compared to WT, although higher k_1 values were observed for the c.911G>A, (p.Arg304Gln) variant. In affected individuals, the variants would be expressed with WT-KCNB2 in a heterozygous manner. We therefore tested the effect on co-expression. While the effects were similar, the voltage dependence and slope of activation was attenuated in the heteromeric as opposed to homomeric expression. This is indicative of difference in activation properties of c.911G>A, (p.Arg304Gln), c.994T>G, (p.Tyr332Asp) and c.1141A>G, (p.Thr381Ala) as compared to WT, but it is notable that the effects were not conserved throughout the mutants nor were the effects consistent among the variants.

KCNB2 **variants show no effect on reversal potential of the channel.**

We next investigated if the mutations in KCNB2 affect the reversal potential of the channel. To do this, we looked at currents evoked by the deactivation protocol illustrated in Fig.4A under conditions of high external $NMDG^+/Na^+$ and low K^+ and high internal K^+ and low $NMDG^+/Na^+$. The deactivation protocol involves channel opening of the variants at +50 mV followed by the deactivation of the channel at different voltages ranging from +50 mV to -120 mV. The raw traces shown in Fig.4B are representative of an oocyte expressing WT-KCNB2. The ensuing current voltage relationship from this protocol leads to the determination of the reversal potential of the

channel, representative of the voltage with no net current. As shown in Fig. 4C and D, the reversal potential of all *KCNB2* variants lies between -60 to -80 mV (Table S3), which is closer to the equilibrium potential of K^+. These results indicate that potassium conductivity by the variants is unaffected in the presence of Na^+ or $NMDG^+$ both extra- and intracellularly.

KCNB2 variants show greater extent of inactivation when compared to WT-KCNB2

Many Kv channels undergo inactivation either during subthreshold depolarization (referred to as closed state inactivation) or during suprathreshold membrane depolarization (referred to as open-state inactivation)[56]. *Shab*-related KCNB channels are characterised by slow inactivation that strongly influences duration of action potentials during repetitive high frequency firing of different neuronal subsets. To assess voltage dependence and extent of this inactivation, we employed the protocol illustrated in Fig. 5A; the bold lines in the protocol correspond to the raw traces shown in Fig. 5B and C when the variants are expressed either alone or with WT-KCNB2, respectively. Both WT-KCNB2 and the variants exhibit slow inactivation as described previously[17,57] during sustained depolarizations at +40 mV for up to 20 s.

We next assessed and compared voltage-dependence of inactivation of WT-KCNB2 and the variants. All *KCNB2* variants exhibit U-shaped inactivation profiles (Fig. 5D and E) as described previously[56,58]. Such profiles are indicative of increased inactivation at negative potentials, which is overcome by channel opening at more depolarized potentials because of increased open probability. To determine the mean free energy required to trigger closed state inactivation, we fitted the data between -150 mV to 10 mV with the sum of two Boltzmann's equations. As compared to WT, most-variants, when co-expressed with WT, show a shift to hyperpolarized

potentials of the inactivation characteristics (Fig.5E and Table 3). These effects are even more pronounced when the variants are expressed in the absence of WT, indicating these amino acid substitutions contribute to voltage dependency of inactivation (Fig.5D and Table 3). Most variants also showed an increase in the slope factors of the Boltzmann relations k_1 and k_2 (Table 3), especially c.911G>A, (p.Arg304Gln). The slope factors k can be written as ratio of thermal energy and electrical energy per Volt (RT/zF with R: universal gas constant, T: temperature, z the apparent gating charge and F the Faraday constant), indicating that, in these variants, the apparent electrical charge z driving inactivation was reduced. By comparing the extent of inactivation exhibited by the variants with respect to WT (Fig. 5F), most variants showed increased inactivation with the exception of c.1141A>G, (p.Thr381Ala). c.994T>G, (p.Tyr332Asp), when expressed alone, showed the greatest extent of inactivation (~35% more inactivation as WT, Fig.5F). It was remarkable, however, that this effect disappeared in the presence of WT-KCNB2.

Similar to the activation kinetics, where c.1141A>G, (p.Thr381Ala) showed a distinct phenotype with fast inactivation at high depolarizations, this variant showed a behaviour distinct to the other variants that we characterized. c.1141A>G, (p.Thr381Ala) opens transiently followed by quick inactivation to a new baseline (Fig. 3A). To check if this variant persists in this inactivated state, we kept the channel open for longer time with our inactivation protocol. As shown in the raw traces represented in Fig. 5G, oocytes expressing WT-KCNB2 (black trace) showed increasing inactivation with time whereas oocytes expressing the c.1141A>G, (p.Thr381Ala) variant did not show inactivation in addition to the rapid inactivation of the open state (blue trace, Fig. 5G, zoomed in Fig.5H) in the 20s post opening of the channel. In contrast, c.1141A>G, (p.Thr381Ala)increases in current indicating that channels are recovered from inactivation (Fig. 5I, *cf.* dashed WT black fit from Fig. 5D and E to c.1141A>G, (p.Thr381Ala) blue data points). The data suggests that

there are two types of inactivation in the c.1141A>G, (p.Thr381Ala) mutant, closed state inactivation – typical for KCNB2 – and a very rapid open state inactivation. Because of the rapid open state inactivation, we cannot clearly determine how many channels are expressed, which explains the low currents observed in Fig. 3A. The rapid inactivation is abolished when co-expressed with WT-KCNB2. The heteromers exhibited activation amplitudes (Fig. 3D) and extent of inactivation (Fig. 5F) similar to those expressing WT alone (Tables 2 and 3).

In contrast to activation and functional expression, that resulted in variable phenotypes among the variants, an increased inactivation, both in voltage dependence and extent, was common to all variants studied in this work. This communality emphasizes the importance of channel inactivation for the development of the disease.

Discussion

Human homologues of the Drosophila *shab* family are the KCNB family of voltage-gated potassium channels that contain two known members: KCNB1 and KCNB2. Variants in the *KCNB1* gene have been identified in individuals suffering from early onset developmental and epileptic encephalopathies[23]. In this study, we identified several variants in the *KCNB2* gene clinically and from the Epi25 and other epilepsy cohorts. This study is the first to identify a channelopathy due to genetic alterations in *KCNB2*. The variants identified clinically are in children and are mostly *de novo* (except for c.1937C>T, (p.Ala646Val) which is inherited). Individuals harboring these variants exhibit a wide array of neurological disorders. Most individuals exhibit delays in either global development, motor milestones or speech/language. These individuals also displayed intellectual disabilities and different dysmorphisms. Dysmorphic facial features were variable across individuals, with synophrys and broad forehead being most

366 common. Functional characterization of the KCNB2 variants revealed a unifying feature: all
367 variants have reduced KCNB2 channel function achieved either by reduced functional expression
368 (c.641C>T, (p.Thr214Met), c.994T>G, (p.Tyr332Asp) and c.1141A>G, (p.Thr381Ala)) and by
369 increased extent of inactivation occurring at more hyperpolarized potentials compared to WT. We,
370 therefore, provide a compelling etiological basis for the onset of the neurological disorders in
371 individuals with mutations in KCNB2.

372 KCNB channels are delayed rectifying channels, i.e., the channels activate and conduct K^+ under
373 depolarized membrane potentials and undergo slow inactivation. Activation and inactivation of
374 KCNB channels, like most Kv channels, are regulated by two mechanisms governed by structural
375 rearrangements of the protein referred to as "gating": activation gating and inactivation gating[59].
376 Activation gating occurs when voltage sensing S1-S4 domains of Kv channels sense membrane
377 depolarization and undergo conformational changes. These structural changes are communicated
378 to the pore domain by electromechanical coupling that leads to pore opening and channel
379 conductance[60]. Inactivation gating involves structural transitions of Kv channels that act as
380 intrinsic negative feedback to inhibit channel conductance and thereby availability, leading to
381 modulation of cellular excitability. Kv2 channels exhibit U-type inactivation arising from pre-open
382 activated but non-conductive channel states[58]. Such inactivation profiles entail a lower degree of
383 inactivation at more depolarized potentials (hence the U-shape of voltage dependence).

384 One of the variants with the most severe disease phenotype is the **c.1141A>G, (p.Thr381Ala)**.
385 The individual (Proband 1, Fig. 1 and Table 1) harboring this variant suffers from global
386 developmental delay with intellectual disability, seizures, and diabetes (for more information,
387 please refer to Supplemental Note: Case Reports). Electrophysiological properties of the variant

corroborate with the severity of the disease. When expressed alone, the current amplitude of the c.1141A>G, (p.Thr381Ala) variant is ~10% of that of WT (Fig. 3B and Fig. 5G) and is rescued when this variant is co-expressed with WT (Fig. 3D). Significant changes in activation midpoint of this variant are seen when expressed either alone or with WT (~20 and 5 mV shift in $V_{50(1)}$ to hyperpolarized potentials, respectively) and slope factor (increase in k_1) is observed (Fig. 3C and E and Table 2). As mentioned above, normalised current-voltage relationship of inactivation, displayed in Fig. 5I, shows an increased recovery from inactivation with increasing voltage (cf. blue line for c.1141A>G, (p.Thr381Ala) and dashed black fit for WT). This inactivation profile is very similar to other channels that express the equivalent T→A variant. c.1141A>G, (p.Thr381Ala), present in the channel selectivity filter, is the conserved fourth residue of the TXXTXGYG signature sequence present in all K^+ channels[61]. The hydroxyl group of this threonine contributes to one of the four K^+ binding sites in potassium channels[62]. Variants of p.Thr381 equivalent positions in other Kv channels, including the closely related KCNB1, does not produce drastic loss of K^+ conductance as seen with KCNB2[61,63,64]. When the equivalent threonine in bacterial KcsA channel (T75) was mutated to a glycine, the rate of inactivation was slower by ~2 fold[62]. With a substitution to an alanine (identical to c.1141A>G, (p.Thr381Ala) in KCNB2 in this study), KcsA, Kv1.5 [MIM 176267] and Shaker channels all show a loss in C-type inactivation, indicating the importance of p.Thr381 equivalent threonine in these channels in allosteric coupling of the activation gate and the selectivity filter[64]. When Coonen *et al.* modified the equivalent residue to an alanine in KCNB1 (p.Thr377Ala) and Kv3.1 [MIM 176258] (p.Thr400Ala), the channel variants were resistant to inactivation thereby losing their U-shape profile as shown by their WT counterparts[63]. We also observe similar reduced inactivation of WT:p.Thr381Ala channels (Fig.5E, cyan trace). Given the involvement of potassium channels in

411 insulin secretion and the presence of diabetes in other potassium channelopathies (ATP-sensitive
412 ones)[65], it is interesting to note that the individual harboring the c.1141A>G, (p.Thr381Ala)
413 mutation was diagnosed with childhood onset diabetes but was not found to have pancreas islet
414 cell autoantibodies. It remains to be determined if diabetes is strongly associated with KCNB2
415 variants once a larger cohort is established. Previous studies have shown that KCNB2 is expressed
416 in human δ cells of the pancreatic islets[66]. Pharmacological inhibition of KCNB2 currents increase
417 action potential duration and amplitude in these cells[67] that leads to augmented somatostatin
418 secretion and powerful inhibition of insulin secretion from pancreatic β cells[68]. The lack of
419 functional expression of the KCNB2 c.1141A>G, (p.Thr381Ala) could potentially mimic KCNB2
420 inhibition that leads to somatostatin-induced paracrine blocking of insulin secretion and onset of
421 diabetes in the individual harboring this mutation.

422 The affected individual harboring the **c.641C>T, (p.Thr214Met)** mutation (Proband 4, Fig. 1 and
423 Table 1) exhibited delayed language milestones along with mild autistic traits in infancy, myopia
424 and synophrys. p.Thr214 is present in the S1-S2 linker; this linker (by virtue of its length) has been
425 shown in KCNA2 [MIM 176262] to be essential for N-glycosylation that influences their
426 functioning, proper folding and trafficking to cell surface[69,70]. However, the S1-S2 linker
427 glycosylation is not conserved in all Kv channels. The threonine present in position 214 in KCNB2
428 is conserved in all human Kv channels[71]. The c.641C>T, (p.Thr214Met) variant, when expressed
429 alone, leads to complete abrogation of K^+ conductance (Fig. 3A and B). The lack of functional
430 expression is rescued when the c.641C>T, (p.Thr214Met) variant is co-expressed with WT, albeit
431 significantly lower than WT (Fig. 3D, Table 2). Such observations have also been reported in other
432 Kv channels. Synthetic mutations in KCNA4 [MIM 176266] and KCNC1 [MIM 176258] and
433 disease relevant mutations in KCNB1 of equivalent threonine residues caused intracellular

retention of the protein and little to no channel currents[71-73]. An alanine mutation to the equivalent threonine in KCNQ2 [MIM 602235] and KCNQ3 [MIM 602232] also yielded reduced potassium currents with drastic effects on voltage dependence and kinetics of activation and kinetics of deactivation[74].

The individual harboring the **c.994T>G, (p.Tyr332Asp)** (Proband 5, Fig. 1, Table 1 and Supplemental Notes: Case Reports) mutation in KCNB2 exhibited global development delay with intellectual disabilities and facial dysmorphisms. The c.994T>G, (p.Tyr332Asp) mutation occurs in the S4-S5 linker of KCNB2. The S4-S5 linker provides electromechanical coupling between the voltage sensing and pore domains that leads to voltage gating of Kv channel function. The S4-S5 linker is very dynamic; this flexible region present on the intracellular side undergoes conformational rearrangements not only during gating and late gating processes, but also during inactivation of some Kv channels[75-78]. Interestingly, this tyrosine present at the end of S4-S5 linker is conserved only in KCNB1 and KCNB2. These channels undergo slow inactivation as compared to other inactivating Kv channels. The c.994T>G, (p.Tyr332Asp) variant, when expressed alone or with WT, show minor effects on the coupling between the voltage sensor and pore domains; this is evident by the shift in the voltage dependence of conductance to hyperpolarized potentials in this variant compared to WT (Fig. 3 and Table 2). However, the major effect on the c.994T>G, (p.Tyr332Asp) mutation is the extent of inactivation observed in this variant (Fig.5D and 5F), which is the strongest among the mutants studied here (apart from maybe c.1141A>G, (p.Thr381Ala)). This effect on inactivation, however, is lost on co-expression of this variant with WT (Fig. 5E and 5F). This observation indicates a hitherto unappreciated role of the tyrosine residue at positions 328 and 332 respectively in KCNB1 and KCNB2 on the electromechanical coupling of their activation and in the inactivation of these channels.

c.911G>A, (p.Arg304Gln), present in the S4 of KCNB2, is one of many positively charged arginine and lysine residues present in the S4 that mediate sensitivity of the ion channel to voltage fluxes; movement of these positive charges in S4 during membrane depolarization cause conformational changes that lead to the opening of the central channel pore[79,80]. Variants of arginine residues within the S4 of Kv and several other ion channels have been described associated with different channelopathies[23,80,81]. Likewise, the individual harboring the c.911G>A, (p.Arg304Gln) mutation in KCNB2 (Proband 6, Fig. 1, Table 1 and Supplemental Notes: Case Reports) exhibited delayed motor, speech and language milestones along with autism spectrum disorder and ADHD. c.911G>A, (p.Arg304Gln) has significant effect on the slope factor k1 of channel activation (Table 2), in the absence or presence of WT, consistent with a reduction of the apparent gating charge in the S4 voltage sensor. This variant, either when expressed alone or with WT, unsurprisingly show significant and drastic effects of the voltage dependence and extent of inactivation (Fig. 5D-F, Table 3).

One of the variants identified in this study is the **c.1937C>T, (p.Ala646Val)** mutation in the C-terminus of KCNB2. The individual harboring this mutation in KCNB2 (Proband 3, Fig. 1, Table 1 and Supplemental Notes: Case Reports) displayed onset of regression/neurodegenerative disease along with delayed motor, speech and language milestones. The c.1937C>T, (p.Ala646Val) variant, when co-expressed with WT or alone, increased inactivation and altered voltage dependence of inactivation (Fig. 5F, Table 3). The **c.281G>A, (p.Gly94Glu)** mutation was identified in an individual (Proband 2, Fig. 1, Table 1 and Supplemental Notes: Case Reports) with developmental and speech delay along with hypotonia and ataxia cerebral palsy. The other N-terminus variant is the c.472A>G, (p.Thr158Ala) identified in two individuals with non-acquired focal epilepsy from the Epi25k exome study. Both the N-terminus variants show increase in extent

of inactivation, especially when expressed with WT (Fig. 5F). There is no precedence on the role of the N-terminus on the inactivation of KCNB2. Interestingly, previous work on exchanging N-terminus of KCNB2 with that of Kv4.2 [KCND2, [MIM 605410]] accelerated inactivation of the KCNB2 chimera[82]. p.Gly94 is a glutamate at equivalent positions in Kv4.2 channels, just as one of our variants (c.281G>A, (p.Gly94Glu)). Detailed investigation on the role of both N and C-termini on KCNB2 channel activity is therefore warranted.

p.Ala375, like p.Thr381, is present in the pore domain and is located at the pore-helix preceding the selectivity filter of KCNB2. Variant of this residue to Valine (c.1124C>T, p.Ala375Val) in KCNB2, both in the absence or presence of WT, significantly enhances the extent of inactivation exhibited by these channels (Fig. 5D-F). This variant was identified in an individual with genetic generalized epilepsy from the Epi25 exome study. p.Ala375 is conserved in other Kv channels such as KCNB1, Kv1.5 and Shaker at equivalent positions, but not in KcsA, Kv4s and hERG channels. Introducing mutations at p.Ala375 equivalent positions in hERG-1 channel (p.Thr618Ala in Kv11.1/*KCNH2* [MIM 152427]) and Kv1.5 (p.Ala473Thr in *KCNA5*, [MIM 176267]) alters voltage dependence of inactivation in these channels[83], suggesting the importance of p.Ala375 and analogous regions in the onset of inactivation in numerous Kv channels.

In addition, we characterised the **c.724G>A, (p.Ala242Thr)** variant identified in a an individual with Sudden Unexpected Death in Epilepsy (Leu et al., 2015). p.Ala242 in KCNB2 is present in the S2 interspersed between two negatively charged glutamates at position 237 and 247. These glutamates in KCNB2 and equivalent positions in other ion channels are thought to interact with positive charge amino acids in the S4 voltage sensor during resting and activated channel states[79]. We speculate that amino acid substitutions of p.Ala242 ought to affect the voltage sensing of

KCNB2. This is evident in the significant changes in slope factors of the voltage-dependence of inactivation in KCNB2-p.Ala242Thr (with or without WT, Table 3) although no changes were observed in activation-voltage relationship of this variant as compared to WT (Fig. 2B-E, Table 2). Of note, p.Ala242 is conserved in KCNB1 but is replaced by other non-polar aliphatic amino acids in other Kv channels such as Shaker or Kv1.5 (Isoleucine at equivalent positions) or Kv4s (Leucine/Methionine).

Finally, we identified a seventh individual (Proband 7, Fig. 1, Table 1 and Supplemental Notes: Case Reports) harboring a c.827C>T, (p.Pro276Leu) mutation during the revision of this manuscript. It is inherited from an unaffected mosaic father, with the variant present in 10% of the reads in blood DNA.. The patient exhibited global developmental delay with moderate intellectual disability, refractory epilepsy and some behavioral issues. He is being treated with multiple anti-seizure medications (for more information, please refer to Supplemental Note: Case Reports). Brain MRI of this patient showed prominent perivascular spaces.

Conclusions

We report variants in *KCNB2* that are associated with a range of neurological disorders including autism and epilepsy. We show strong evidence that the *de novo KCNB2* variants cause neurodevelopmental disorders and that these variants either significantly i) reduce the currents generated by these Kv channels, or ii) shift the voltage dependence of inactivation to hyperpolarized membranes and increase the extent of inactivation as compared to WT. inactivation, in general, is a cumulative effect that is most impactful when trains of stimulations do not allow for recovery from inactivation before the next stimulus[58]. The effect is a reduction of the available functional KCNB2 channels that shapes the duration and interspike intervals of action

potentials, leading to changes in cellular excitability in neurons that express these variants. Further experiments in native systems are warranted to corroborate this hypothesis, which provides the underlying etiological basis of how KCNB2 dysfunction causes disease. Despite variation in the associated diseases, it is remarkable that all variants had a common underlying phenotype on the molecular level.

Declaration of interests

The authors declare no competing interests.

Data and code availability

The published article includes all datasets generated or analyzed during this study, apart from exome sequencing data which are not publicly available due to privacy restrictions. All experimental data will be freely available upon request from the corresponding authors.

Acknowledgments

This work was financially supported by the Canadian Institutes for Health Research (PJT-169160 to R.B.) and the Natural Sciences and Engineering Research Council of Canada (RGPIN-2023-04752 to RB). CIRCA is a research center financially supported by the Fonds de recherche Québec — Santé. For simulations, computational resources were provided by the Digital Research Alliance of Canada. SMS is supported by the UK Epilepsy Society. Part of this work was undertaken at University College London Hospitals, which received a proportion of funding from the NIHR Biomedical Research Centres funding scheme. We would like to thank Nassima

Addour-Boudrahem and the C4R-SOLVE study staff at the Children's Hospital of Eastern Ontario Research Institute, for their contribution to the exome analysis of patient 7. Portions of this work was performed under the Care4Rare Canada Consortium funded by Genome Canada and the Ontario Genomics Institute (OGI-147), the Canadian Institutes of Health Research, Ontario Research Fund, Genome Alberta, Genome British Columbia, Genome Quebec, and Children's Hospital of Eastern Ontario Foundation.

Author contributions

The study was designed by S.B., J.R., R.B and P.M.C. The individuals were recruited by C.M.L., J.M.S., R.J.L., K.C., A.L., D.C.K., S.C.R, S.M.S., E.M.M.M.H.V.K., K.K., P.M.V.H., F.D., C.D., B.R.S., A.A., M.S., E.S.T., S.S.H., I.T. and P.M.C. The disease manifestations were summarized and compared by C.M. and P.M.C. The experiments were performed or supervised by S.B., J.R., R.B and P.M.C. The data was analyzed by S.B., J.R., R.B and P.M.C. The draft was written by S.B., J.R., C.M., R.B and P.M.C. All authors contributed to revising the manuscript.

Web resources

gnomAD population database, https://gnomad.broadinstitute.org/

Epi25 exome server: https://epi25.broadinstitute.org/

562

Tables

Table 1. Main clinical features of the affected and phenotyped individuals.

Proband	1	2	3	4	5	6	7
KCNB2 variant (NM_004770.3)	c.1141A>G, (p.Thr381Ala)	c.281G>A, (p.Gly94Glu)	c.1937C>T, (p.Ala646Val)	c.641C>T, (p.Thr214Met)	c.994T>G, (p.Tyr332Asp)	c.911G>A, (p.Arg304Gln)	c.827C>T, (p.Pro276Leu)
Inheritance	*de novo*	*de novo*	Inherited	*de novo*	*de novo*	*de novo*	Mosaic[a]
Sex	Female	Male	Female	Male	Female	Male	Male
Age at last assessment	5 years	2.5 years	3 years	18 years	21 months	9 years	15 years
Medical history							
Brain anomalies (MRI results)	+	N/A	-	N/A	+	N/A	-
Cardiac anomalies	+	+	-	-	N/A	N/A	-
Urogenital anomalies	+	+	-	-	-	-	-
Ophthalmological anomalies	+	+	-	+	+	N/A	-
Growth and Development							
DD	+	+	+	+	+[b]	+	+
ID	+	N/A	+	+	+	+	+
Autistic features	-	N/A[C]	-	mild	N/A[C]	mild	mild
Epilepsy	+[d]	-	-	-	-	-	+[e]
Dysmorphisms							
Facial	+	+	+	-	+	+	-
Hand	-	+	+	-	+	+	-
Synophrys	-	+	-	+	-	-	-
Other features							
Hypotonia	+	+[f]	-	-	-	-	-
ADHD	-	-	-	N/A	-	+	-

Abbreviations are as follows: N/A: not available, DD: developmental delay, ID: Intellectual disability, ADHD: Attention-Deficit / Hyperactivity Disorder, Mosaic[a] - Individual 7 and his father exhibited genetic mosaicism, +[b] - severe, N/A[c] - patient too young to make an autistic spectrum disorder (ASD) diagnosis, +[d] - seizure effectively treated with Levetiracetam, +[e] - multiple anti-seizure medication (refer to supplemental information), +[f] - Hypotonia with Ataxic cerebral palsy. Please refer to supplemental data for detailed case report for each patient.

Table 2. Activation properties of Kv2.2 variants

Variants	Without WT					With WT				
	Current Amplitudes (± S.D.) [µA]	$V_{50(1)}$ (mV)	k_1	$V_{50(2)}$ (mV)	k_2	Current Amplitudes (± S.D.) [µA]	$V_{50(1)}$ (mV)	k_1	$V_{50(2)}$ (mV)	k_2
WT	47.7 ± 14.2	-1.9 ± 5.4	6.7 ± 0.9	24.4 ± 5.9	12.3 ± 2.1	47.7 ± 14.2	-1.9 ± 5.4	6.7 ± 0.9	24.4 ± 5.9	12.3 ± 2.1
p.Gly94Glu	45.8 ± 13.2	-1.6 ± 5.8	6.7 ± 0.6	24.5 ± 4.4	12.3 ± 1.7	46.5 ± 17.7	-1.4 ± 5.2	6.7 ± 0.8	26.1 ± 10.7	12.3 ± 2.4
p.Thr158Ala	44.8 ± 14.7	-5.6 ± 5.9	6.7 ± 0.8	20.4 ± 6.9	12.1 ± 2.0	39.1 ± 12.6	-2.2 ± 5.7	6.8 ± 0.6	26.3 ± 8.2	13.8 ± 2.3
p.Thr214Met	2.1 ± 2.6***	n.a.				31.8 ± 7.9*	5.0 ± 2.9	7.5 ± 0.6	34.6 ± 4.8*	13.5 ± 1.6
p.Ala242Thr	37.7 ± 10.3	-6.6 ± 3.5	6.7 ± 0.5	18.8 ± 5.6	12.3 ± 1.4	44.5 ± 11.6	-3.9 ± 5.4	6.6 ± 0.5	21.8 ± 7.6	11.8 ± 1.9
p.Arg304Gln	40.6 ± 11.8	-1.2 ± 3.0	8.2 ± 0.9**	26.6 ± 5.0	13.4 ± 2.1	35.8 ± 6.9	0.8 ± 3.9	7.7 ± 0.4*	27.4 ± 5.2	12.9 ± 1.0
p.Tyr332Asp	25.5 ± 5.9**	7.6 ± 3.2**	7.1 ± 0.6	36.4 ± 5.2**	13.9 ± 1.6	48.5 ± 5.7	4.4 ± 2.8	7.0 ± 1.1	30.3 ± 5.3	10.8 ± 1.8
p.Ala375Val	39.9 ± 5.2	-6.4 ± 4.4	7.5 ± 0.9	25.7 ± 6.4	14.0 ± 2.9	43.1 ± 10.8	-3.3 ± 6.2	7.2 ± 0.9	26.5 ± 9.2	13.8 ± 2.2
p.Thr381Ala	7.9 ± 3.7***	-22.7 ± 5.9***	14.3 ± 0.9***	59.1 ± 6.4***	14.0 ± 3.6	44.1 ± 12.4	-7.3 ± 1.6*	10.3 ± 1.3***	26.1 ± 9.1	12.0 ± 4.9
p.Ala646Val	44.2 ± 10.0	-3.3 ± 2.3	6.7 ± 0.6	22.7 ± 3.3	13.3 ± 1.7	42.4 ± 12.9	1.5 ± 5.1	6.2 ± 0.7	27.8 ± 5.5	10.9 ± 1.8

* p<0.05, **p<0.01, *** p<0.001 via Kruskal Wallis one-way ANOVA with post hoc correction for multiple comparisons with Dunn's post-hoc test.

n.a. - not analysed; the amplitudes were too low to determine activation properties.

Table 3. Inactivation properties of Kv2.2 variants

Variants	Without WT				With WT			
	$V_{50(1)}$ (mV)	k_1	$V_{50(2)}$ (mV)	k_2	$V_{50(1)}$ (mV)	k_1	$V_{50(2)}$ (mV)	k_2
WT	-51.3 ± 11.1	11.6 ± 5.0	-19.9 ± 4.0	6.5 ± 1.6	-51.3 ± 11.1	11.6 ± 5.0	-19.9 ± 4.0	6.5 ± 1.6
p.Gly94Glu	-46.9 ± 10.83	10.7 ± 4.9	-23.5 ± 4.7	5.1 ± 0.8	-41.3 ± 13.4	9.8 ± 5.0	-24.0 ± 4.0	4.5 ± 0.9
p.Thr158Ala	-58.7 ± 10.3	11.9 ± 3.4	-29.5 ± 4.4*	5.7 ± 1.7	-59.1 ± 10.9	13.5 ± 3.7	-29.2 ± 9.5	5.5 ± 0.8
p.Thr214Met	n.a.				-34.6 ± 5.0	7.0 ± 2.1	-18.5 ± 0.8	4.7 ± 1.1
p.Ala242Thr	-59.3 ± 5.9	18.1 ± 1.8*	-30.4 ± 2.2*	6.4 ± 0.5	-57.1 ± 16.1	15.4 ± 2.7	-25.3 ± 3.8	6.2 ± 1.4
p.Arg304Gln	-82.9 ± 12.8**	14.6 ± 2.5	-37.8 ± 4.5***	7.1 ± 1.5	-67.4 ± 11.3	18.8 ± 2.1*	-27.6 ± 3.1	6.8 ± 0.5
p.Tyr332Asp	-34.1 ± 11.9	6.5 ± 2.5	-16.8 ± 4.9	4.3 ± 1.0*	-23.0 ± 3.6*	5.3 ± 2.1	-11.0 ± 0.9	4.0 ± 0.9*
p.Ala375Val	-52.1 ± 9.4	9.7 ± 3.2	-34.0 ± 4.2***	3.9 ± 1.0**	-54.3 ± 10.3	15.0 ± 5.2	-29.8 ± 4.3*	6.0 ± 1.6
p.Thr381Ala	n.a.				-60.0 ± 11.5	12.1 ± 3.4	-30.4 ± 7.2*	6.1 ± 1.1
p.Ala646Val	-64.7 ± 14.2	16.2 ± 3.9	-29.8 ± 6.7	6.2 ± 0.8	-61.3 ± 9.0	13.3 ± 2.2	-28.3 ± 3.0	6.0 ± 0.8

* $p<0.05$, ** $p<0.01$, *** $p<0.001$ via Kruskal Wallis one-way ANOVA with post hoc correction for multiple comparisons with Dunn's post-hoc test.

n.a. - not analysed; the amplitudes were too low in p.Thr214Met and recovery from inactivation was seen in p.Thr381Ala that prevented determination of their inactivation properties.

References

1. Misonou, H., and Trimmer, J.S. (2004). Determinants of voltage-gated potassium channel surface expression and localization in Mammalian neurons. Crit Rev Biochem Mol Biol *39*, 125-145. 10.1080/10409230490475417.
2. Johnson, B., Leek, A.N., and Tamkun, M.M. (2019). Kv2 channels create endoplasmic reticulum / plasma membrane junctions: a brief history of Kv2 channel subcellular localization. Channels (Austin) *13*, 88-101. 10.1080/19336950.2019.1568824.
3. Kihira, Y., Hermanstyne, T.O., and Misonou, H. (2010). Formation of heteromeric Kv2 channels in mammalian brain neurons. J Biol Chem *285*, 15048-15055. 10.1074/jbc.M109.074260.
4. Trimmer, J.S. (1991). Immunological identification and characterization of a delayed rectifier K+ channel polypeptide in rat brain. Proc Natl Acad Sci U S A *88*, 10764-10768. 10.1073/pnas.88.23.10764.
5. Murakoshi, H., and Trimmer, J.S. (1999). Identification of the Kv2.1 K+ channel as a major component of the delayed rectifier K+ current in rat hippocampal neurons. J Neurosci *19*, 1728-1735. 10.1523/JNEUROSCI.19-05-01728.1999.
6. Hwang, P.M., Fotuhi, M., Bredt, D.S., Cunningham, A.M., and Snyder, S.H. (1993). Contrasting immunohistochemical localizations in rat brain of two novel K+ channels of the Shab subfamily. J Neurosci *13*, 1569-1576. 10.1523/JNEUROSCI.13-04-01569.1993.
7. Guan, D., Tkatch, T., Surmeier, D.J., Armstrong, W.E., and Foehring, R.C. (2007). Kv2 subunits underlie slowly inactivating potassium current in rat neocortical pyramidal neurons. J Physiol *581*, 941-960. 10.1113/jphysiol.2007.128454.
8. Lim, S.T., Antonucci, D.E., Scannevin, R.H., and Trimmer, J.S. (2000). A novel targeting signal for proximal clustering of the Kv2.1 K+ channel in hippocampal neurons. Neuron *25*, 385-397. 10.1016/s0896-6273(00)80902-2.
9. Bishop, H.I., Guan, D., Bocksteins, E., Parajuli, L.K., Murray, K.D., Cobb, M.M., Misonou, H., Zito, K., Foehring, R.C., and Trimmer, J.S. (2015). Distinct Cell- and Layer-Specific Expression Patterns and Independent Regulation of Kv2 Channel Subtypes in Cortical Pyramidal Neurons. J Neurosci *35*, 14922-14942. 10.1523/JNEUROSCI.1897-15.2015.
10. Trimmer, J.S. (2015). Subcellular localization of K+ channels in mammalian brain neurons: remarkable precision in the midst of extraordinary complexity. Neuron *85*, 238-256. 10.1016/j.neuron.2014.12.042.
11. Johnston, J., Griffin, S.J., Baker, C., Skrzypiec, A., Chernova, T., and Forsythe, I.D. (2008). Initial segment Kv2.2 channels mediate a slow delayed rectifier and maintain high frequency action potential firing in medial nucleus of the trapezoid body neurons. J Physiol *586*, 3493-3509. 10.1113/jphysiol.2008.153734.
12. Hermanstyne, T.O., Kihira, Y., Misono, K., Deitchler, A., Yanagawa, Y., and Misonou, H. (2010). Immunolocalization of the voltage-gated potassium channel Kv2.2 in GABAergic neurons in the basal forebrain of rats and mice. J Comp Neurol *518*, 4298-4310. 10.1002/cne.22457.
13. Hermanstyne, T.O., Subedi, K., Le, W.W., Hoffman, G.E., Meredith, A.L., Mong, J.A., and Misonou, H. (2013). Kv2.2: a novel molecular target to study the role of basal forebrain GABAergic neurons in the sleep-wake cycle. Sleep *36*, 1839-1848. 10.5665/sleep.3212.

14. Regnier, G., Bocksteins, E., Van de Vijver, G., Snyders, D.J., and van Bogaert, P.P. (2016). The contribution of Kv2.2-mediated currents decreases during the postnatal development of mouse dorsal root ganglion neurons. Physiol Rep *4*. 10.14814/phy2.12731.
15. Johnston, J., Forsythe, I.D., and Kopp-Scheinpflug, C. (2010). Going native: voltage-gated potassium channels controlling neuronal excitability. J Physiol *588*, 3187-3200. 10.1113/jphysiol.2010.191973.
16. Tsantoulas, C., and McMahon, S.B. (2014). Opening paths to novel analgesics: the role of potassium channels in chronic pain. Trends Neurosci *37*, 146-158. 10.1016/j.tins.2013.12.002.
17. Du, J., Haak, L.L., Phillips-Tansey, E., Russell, J.T., and McBain, C.J. (2000). Frequency-dependent regulation of rat hippocampal somato-dendritic excitability by the K+ channel subunit Kv2.1. J Physiol *522 Pt 1*, 19-31. 10.1111/j.1469-7793.2000.t01-2-00019.xm.
18. Malin, S.A., and Nerbonne, J.M. (2002). Delayed rectifier K+ currents, IK, are encoded by Kv2 alpha-subunits and regulate tonic firing in mammalian sympathetic neurons. J Neurosci *22*, 10094-10105. 10.1523/JNEUROSCI.22-23-10094.2002.
19. Mohapatra, D.P., Misonou, H., Pan, S.J., Held, J.E., Surmeier, D.J., and Trimmer, J.S. (2009). Regulation of intrinsic excitability in hippocampal neurons by activity-dependent modulation of the KV2.1 potassium channel. Channels (Austin) *3*, 46-56. 10.4161/chan.3.1.7655.
20. Tsantoulas, C., Zhu, L., Yip, P., Grist, J., Michael, G.J., and McMahon, S.B. (2014). Kv2 dysfunction after peripheral axotomy enhances sensory neuron responsiveness to sustained input. Exp Neurol *251*, 115-126. 10.1016/j.expneurol.2013.11.011.
21. Bocksteins, E. (2016). Kv5, Kv6, Kv8, and Kv9 subunits: No simple silent bystanders. J Gen Physiol *147*, 105-125. 10.1085/jgp.201511507.
22. Pongs, O., and Schwarz, J.R. (2010). Ancillary subunits associated with voltage-dependent K+ channels. Physiol Rev *90*, 755-796. 10.1152/physrev.00020.2009.
23. Bar, C., Barcia, G., Jennesson, M., Le Guyader, G., Schneider, A., Mignot, C., Lesca, G., Breuillard, D., Montomoli, M., Keren, B., et al. (2020). Expanding the genetic and phenotypic relevance of KCNB1 variants in developmental and epileptic encephalopathies: 27 new patients and overview of the literature. Hum Mutat *41*, 69-80. 10.1002/humu.23915.
24. Torkamani, A., Bersell, K., Jorge, B.S., Bjork, R.L., Jr., Friedman, J.R., Bloss, C.S., Cohen, J., Gupta, S., Naidu, S., Vanoye, C.G., et al. (2014). De novo KCNB1 mutations in epileptic encephalopathy. Ann Neurol *76*, 529-540. 10.1002/ana.24263.
25. Calhoun, J.D., Vanoye, C.G., Kok, F., George, A.L., Jr., and Kearney, J.A. (2017). Characterization of a KCNB1 variant associated with autism, intellectual disability, and epilepsy. Neurol Genet *3*, e198. 10.1212/NXG.0000000000000198.
26. Saitsu, H., Akita, T., Tohyama, J., Goldberg-Stern, H., Kobayashi, Y., Cohen, R., Kato, M., Ohba, C., Miyatake, S., Tsurusaki, Y., et al. (2015). De novo KCNB1 mutations in infantile epilepsy inhibit repetitive neuronal firing. Sci Rep *5*, 15199. 10.1038/srep15199.
27. Thiffault, I., Speca, D.J., Austin, D.C., Cobb, M.M., Eum, K.S., Safina, N.P., Grote, L., Farrow, E.G., Miller, N., Soden, S., et al. (2015). A novel epileptic encephalopathy mutation in KCNB1 disrupts Kv2.1 ion selectivity, expression, and localization. J Gen Physiol *146*, 399-410. 10.1085/jgp.201511444.
28. Speca, D.J., Ogata, G., Mandikian, D., Bishop, H.I., Wiler, S.W., Eum, K., Wenzel, H.J., Doisy, E.T., Matt, L., Campi, K.L., et al. (2014). Deletion of the Kv2.1 delayed rectifier

potassium channel leads to neuronal and behavioral hyperexcitability. Genes Brain Behav *13*, 394-408. 10.1111/gbb.12120.

29. Hawkins, N.A., Misra, S.N., Jurado, M., Kang, S.K., Vierra, N.C., Nguyen, K., Wren, L., George, A.L., Jr., Trimmer, J.S., and Kearney, J.A. (2021). Epilepsy and neurobehavioral abnormalities in mice with a dominant-negative KCNB1 pathogenic variant. Neurobiol Dis *147*, 105141. 10.1016/j.nbd.2020.105141.
30. Campeau, P.M., Kasperaviciute, D., Lu, J.T., Burrage, L.C., Kim, C., Hori, M., Powell, B.R., Stewart, F., Felix, T.M., van den Ende, J., et al. (2014). The genetic basis of DOORS syndrome: an exome-sequencing study. Lancet Neurol *13*, 44-58. 10.1016/S1474-4422(13)70265-5.
31. Hunter, J.M., Massingham, L.J., Manickam, K., Bartholomew, D., Williamson, R.K., Schwab, J.L., Marhabaie, M., Siemon, A., de Los Reyes, E., Reshmi, S.C., et al. (2022). Inherited and de novo variants extend the etiology of TAOK1-associated neurodevelopmental disorder. Cold Spring Harb Mol Case Stud *8*. 10.1101/mcs.a006180.
32. Cohen, A.S.A., Farrow, E.G., Abdelmoity, A.T., Alaimo, J.T., Amudhavalli, S.M., Anderson, J.T., Bansal, L., Bartik, L., Baybayan, P., Belden, B., et al. (2022). Genomic answers for children: Dynamic analyses of >1000 pediatric rare disease genomes. Genet Med *24*, 1336-1348. 10.1016/j.gim.2022.02.007.
33. Chevarin, M., Duffourd, Y., R, A.B., Moutton, S., Lecoquierre, F., Daoud, F., Kuentz, P., Cabret, C., Thevenon, J., Gautier, E., et al. (2020). Excess of de novo variants in genes involved in chromatin remodelling in patients with marfanoid habitus and intellectual disability. J Med Genet *57*, 466-474. 10.1136/jmedgenet-2019-106425.
34. Schwantje, M., de Sain-van der Velden, M., Jans, J., van Gassen, K., Dorrepaal, C., Koop, K., and Visser, G. (2019). Genetic defect of the sodium-dependent multivitamin transporter: A treatable disease, mimicking biotinidase deficiency. JIMD Rep *48*, 11-14. 10.1002/jmd2.12040.
35. Stolerman, E.S., Francisco, E., Stallworth, J.L., Jones, J.R., Monaghan, K.G., Keller-Ramey, J., Person, R., Wentzensen, I.M., McWalter, K., Keren, B., et al. (2019). Genetic variants in the KDM6B gene are associated with neurodevelopmental delays and dysmorphic features. Am J Med Genet A *179*, 1276-1286. 10.1002/ajmg.a.61173.
36. Hamilton, A., Tetreault, M., Dyment, D.A., Zou, R., Kernohan, K., Geraghty, M.T., Consortium, F.C., Care4Rare Canada, C., Hartley, T., and Boycott, K.M. (2016). Concordance between whole-exome sequencing and clinical Sanger sequencing: implications for patient care. Mol Genet Genomic Med *4*, 504-512. 10.1002/mgg3.223.
37. Boycott, K.M., Azzariti, D.R., Hamosh, A., and Rehm, H.L. (2022). Seven years since the launch of the Matchmaker Exchange: The evolution of genomic matchmaking. Hum Mutat *43*, 659-667. 10.1002/humu.24373.
38. Bossi, E., Fabbrini, M.S., and Ceriotti, A. (2007). Exogenous protein expression in Xenopus oocytes: basic procedures. Methods Mol Biol *375*, 107-131. 10.1007/978-1-59745-388-2_6.
39. Stefani, E., and Bezanilla, F. (1998). Cut-open oocyte voltage-clamp technique. Methods Enzymol *293*, 300-318. 10.1016/s0076-6879(98)93020-8.
40. Long, S.B., Tao, X., Campbell, E.B., and MacKinnon, R. (2007). Atomic structure of a voltage-dependent K+ channel in a lipid membrane-like environment. Nature *450*, 376-382. 10.1038/nature06265.

41. Jumper, J., Evans, R., Pritzel, A., Green, T., Figurnov, M., Ronneberger, O., Tunyasuvunakool, K., Bates, R., Zidek, A., Potapenko, A., et al. (2021). Highly accurate protein structure prediction with AlphaFold. Nature *596*, 583-589. 10.1038/s41586-021-03819-2.
42. Brooks, B.R., Brooks, C.L., 3rd, Mackerell, A.D., Jr., Nilsson, L., Petrella, R.J., Roux, B., Won, Y., Archontis, G., Bartels, C., Boresch, S., et al. (2009). CHARMM: the biomolecular simulation program. J Comput Chem *30*, 1545-1614. 10.1002/jcc.21287.
43. Jo, S., Kim, T., Iyer, V.G., and Im, W. (2008). CHARMM-GUI: a web-based graphical user interface for CHARMM. J Comput Chem *29*, 1859-1865. 10.1002/jcc.20945.
44. Lee, J., Cheng, X., Swails, J.M., Yeom, M.S., Eastman, P.K., Lemkul, J.A., Wei, S., Buckner, J., Jeong, J.C., Qi, Y., et al. (2016). CHARMM-GUI Input Generator for NAMD, GROMACS, AMBER, OpenMM, and CHARMM/OpenMM Simulations Using the CHARMM36 Additive Force Field. J Chem Theory Comput *12*, 405-413. 10.1021/acs.jctc.5b00935.
45. Phillips, J.C., Hardy, D.J., Maia, J.D.C., Stone, J.E., Ribeiro, J.V., Bernardi, R.C., Buch, R., Fiorin, G., Henin, J., Jiang, W., et al. (2020). Scalable molecular dynamics on CPU and GPU architectures with NAMD. J Chem Phys *153*, 044130. 10.1063/5.0014475.
46. Kortum, F., Caputo, V., Bauer, C.K., Stella, L., Ciolfi, A., Alawi, M., Bocchinfuso, G., Flex, E., Paolacci, S., Dentici, M.L., et al. (2015). Mutations in KCNH1 and ATP6V1B2 cause Zimmermann-Laband syndrome. Nat Genet *47*, 661-667. 10.1038/ng.3282.
47. Bauer, C.K., Schneeberger, P.E., Kortum, F., Altmuller, J., Santos-Simarro, F., Baker, L., Keller-Ramey, J., White, S.M., Campeau, P.M., Gripp, K.W., and Kutsche, K. (2019). Gain-of-Function Mutations in KCNN3 Encoding the Small-Conductance Ca(2+)-Activated K(+) Channel SK3 Cause Zimmermann-Laband Syndrome. Am J Hum Genet *104*, 1139-1157. 10.1016/j.ajhg.2019.04.012.
48. Beauregard-Lacroix, E., Pacheco-Cuellar, G., Ajeawung, N.F., Tardif, J., Dieterich, K., Dabir, T., Vind-Kezunovic, D., White, S.M., Zadori, D., Castiglioni, C., et al. (2021). DOORS syndrome and a recurrent truncating ATP6V1B2 variant. Genet Med *23*, 149-154. 10.1038/s41436-020-00950-9.
49. Leu, C., Balestrini, S., Maher, B., Hernandez-Hernandez, L., Gormley, P., Hamalainen, E., Heggeli, K., Schoeler, N., Novy, J., Willis, J., et al. (2015). Genome-wide Polygenic Burden of Rare Deleterious Variants in Sudden Unexpected Death in Epilepsy. EBioMedicine *2*, 1063-1070. 10.1016/j.ebiom.2015.07.005.
50. Epi, C., Chen, S., Neale, B.M., and Berkovic, S.F. (2023). Shared and distinct ultra-rare genetic risk for diverse epilepsies: A whole-exome sequencing study of 54,423 individuals across multiple genetic ancestries. medRxiv. 10.1101/2023.02.22.23286310.
51. Tavtigian, S.V., Harrison, S.M., Boucher, K.M., and Biesecker, L.G. (2020). Fitting a naturally scaled point system to the ACMG/AMP variant classification guidelines. Hum Mutat *41*, 1734-1737. 10.1002/humu.24088.
52. Kopanos, C., Tsiolkas, V., Kouris, A., Chapple, C.E., Albarca Aguilera, M., Meyer, R., and Massouras, A. (2019). VarSome: the human genomic variant search engine. Bioinformatics *35*, 1978-1980. 10.1093/bioinformatics/bty897.
53. Lek, M., Karczewski, K.J., Minikel, E.V., Samocha, K.E., Banks, E., Fennell, T., O'Donnell-Luria, A.H., Ware, J.S., Hill, A.J., Cummings, B.B., et al. (2016). Analysis of protein-coding genetic variation in 60,706 humans. Nature *536*, 285-291. 10.1038/nature19057.

54. Wiel, L., Baakman, C., Gilissen, D., Veltman, J.A., Vriend, G., and Gilissen, C. (2019). MetaDome: Pathogenicity analysis of genetic variants through aggregation of homologous human protein domains. Hum Mutat *40*, 1030-1038. 10.1002/humu.23798.
55. McLaren, W., Gil, L., Hunt, S.E., Riat, H.S., Ritchie, G.R., Thormann, A., Flicek, P., and Cunningham, F. (2016). The Ensembl Variant Effect Predictor. Genome Biol *17*, 122. 10.1186/s13059-016-0974-4.
56. Bahring, R., Barghaan, J., Westermeier, R., and Wollberg, J. (2012). Voltage sensor inactivation in potassium channels. Front Pharmacol *3*, 100. 10.3389/fphar.2012.00100.
57. Schmalz, F., Kinsella, J., Koh, S.D., Vogalis, F., Schneider, A., Flynn, E.R., Kenyon, J.L., and Horowitz, B. (1998). Molecular identification of a component of delayed rectifier current in gastrointestinal smooth muscles. Am J Physiol *274*, G901-911. 10.1152/ajpgi.1998.274.5.G901.
58. Klemic, K.G., Shieh, C.C., Kirsch, G.E., and Jones, S.W. (1998). Inactivation of Kv2.1 potassium channels. Biophys J *74*, 1779-1789. 10.1016/S0006-3495(98)77888-9.
59. Kim, D.M., and Nimigean, C.M. (2016). Voltage-Gated Potassium Channels: A Structural Examination of Selectivity and Gating. Cold Spring Harb Perspect Biol *8*. 10.1101/cshperspect.a029231.
60. Blunck, R., and Batulan, Z. (2012). Mechanism of electromechanical coupling in voltage-gated potassium channels. Front Pharmacol *3*, 166. 10.3389/fphar.2012.00166.
61. Heginbotham, L., Lu, Z., Abramson, T., and MacKinnon, R. (1994). Mutations in the K+ channel signature sequence. Biophys J *66*, 1061-1067. 10.1016/S0006-3495(94)80887-2.
62. Matulef, K., Annen, A.W., Nix, J.C., and Valiyaveetil, F.I. (2016). Individual Ion Binding Sites in the K(+) Channel Play Distinct Roles in C-type Inactivation and in Recovery from Inactivation. Structure *24*, 750-761. 10.1016/j.str.2016.02.021.
63. Coonen, L., Mayeur, E., De Neuter, N., Snyders, D.J., Cuello, L.G., and Labro, A.J. (2020). The Selectivity Filter Is Involved in the U-Type Inactivation Process of Kv2.1 and Kv3.1 Channels. Biophys J *118*, 2612-2620. 10.1016/j.bpj.2020.03.032.
64. Labro, A.J., Cortes, D.M., Tilegenova, C., and Cuello, L.G. (2018). Inverted allosteric coupling between activation and inactivation gates in K(+) channels. Proc Natl Acad Sci U S A *115*, 5426-5431. 10.1073/pnas.1800559115.
65. Ashcroft, F.M. (2005). ATP-sensitive potassium channelopathies: focus on insulin secretion. J Clin Invest *115*, 2047-2058. 10.1172/JCI25495.
66. Yan, L., Figueroa, D.J., Austin, C.P., Liu, Y., Bugianesi, R.M., Slaughter, R.S., Kaczorowski, G.J., and Kohler, M.G. (2004). Expression of voltage-gated potassium channels in human and rhesus pancreatic islets. Diabetes *53*, 597-607. 10.2337/diabetes.53.3.597.
67. Braun, M., Ramracheya, R., Amisten, S., Bengtsson, M., Moritoh, Y., Zhang, Q., Johnson, P.R., and Rorsman, P. (2009). Somatostatin release, electrical activity, membrane currents and exocytosis in human pancreatic delta cells. Diabetologia *52*, 1566-1578. 10.1007/s00125-009-1382-z.
68. Li, X.N., Herrington, J., Petrov, A., Ge, L., Eiermann, G., Xiong, Y., Jensen, M.V., Hohmeier, H.E., Newgard, C.B., Garcia, M.L., et al. (2013). The role of voltage-gated potassium channels Kv2.1 and Kv2.2 in the regulation of insulin and somatostatin release from pancreatic islets. J Pharmacol Exp Ther *344*, 407-416. 10.1124/jpet.112.199083.
69. Zhu, J., Watanabe, I., Poholek, A., Koss, M., Gomez, B., Yan, C., Recio-Pinto, E., and Thornhill, W.B. (2003). Allowed N-glycosylation sites on the Kv1.2 potassium channel

S1-S2 linker: implications for linker secondary structure and the glycosylation effect on channel function. Biochem J *375*, 769-775. 10.1042/BJ20030517.

70. Watanabe, I., Zhu, J., Sutachan, J.J., Gottschalk, A., Recio-Pinto, E., and Thornhill, W.B. (2007). The glycosylation state of Kv1.2 potassium channels affects trafficking, gating, and simulated action potentials. Brain Res *1144*, 1-18. 10.1016/j.brainres.2007.01.092.
71. McKeown, L., Burnham, M.P., Hodson, C., and Jones, O.T. (2008). Identification of an evolutionarily conserved extracellular threonine residue critical for surface expression and its potential coupling of adjacent voltage-sensing and gating domains in voltage-gated potassium channels. J Biol Chem *283*, 30421-30432. 10.1074/jbc.M708921200.
72. Marini, C., Romoli, M., Parrini, E., Costa, C., Mei, D., Mari, F., Parmeggiani, L., Procopio, E., Metitieri, T., Cellini, E., et al. (2017). Clinical features and outcome of 6 new patients carrying de novo KCNB1 gene mutations. Neurol Genet *3*, e206. 10.1212/NXG.0000000000000206.
73. Kang, S.K., Vanoye, C.G., Misra, S.N., Echevarria, D.M., Calhoun, J.D., O'Connor, J.B., Fabre, K.L., McKnight, D., Demmer, L., Goldenberg, P., et al. (2019). Spectrum of K(V) 2.1 Dysfunction in KCNB1-Associated Neurodevelopmental Disorders. Ann Neurol *86*, 899-912. 10.1002/ana.25607.
74. Full, Y., Seebohm, G., Lerche, H., and Maljevic, S. (2013). A conserved threonine in the S1-S2 loop of KV7.2 and K V7.3 channels regulates voltage-dependent activation. Pflugers Arch *465*, 797-804. 10.1007/s00424-012-1184-x.
75. Kalstrup, T., and Blunck, R. (2018). S4-S5 linker movement during activation and inactivation in voltage-gated K(+) channels. Proc Natl Acad Sci U S A *115*, E6751-E6759. 10.1073/pnas.1719105115.
76. Barghaan, J., and Bahring, R. (2009). Dynamic coupling of voltage sensor and gate involved in closed-state inactivation of kv4.2 channels. J Gen Physiol *133*, 205-224. 10.1085/jgp.200810073.
77. Isacoff, E.Y., Jan, Y.N., and Jan, L.Y. (1991). Putative receptor for the cytoplasmic inactivation gate in the Shaker K+ channel. Nature *353*, 86-90. 10.1038/353086a0.
78. Ye, W., Zhao, H., Dai, Y., Wang, Y., Lo, Y.H., Jan, L.Y., and Lee, C.H. (2022). Activation and closed-state inactivation mechanisms of the human voltage-gated K(V)4 channel complexes. Mol Cell *82*, 2427-2442 e2424. 10.1016/j.molcel.2022.04.032.
79. Bezanilla, F. (2000). The voltage sensor in voltage-dependent ion channels. Physiol Rev *80*, 555-592. 10.1152/physrev.2000.80.2.555.
80. Catterall, W.A. (2010). Ion channel voltage sensors: structure, function, and pathophysiology. Neuron *67*, 915-928. 10.1016/j.neuron.2010.08.021.
81. Smets, K., Duarri, A., Deconinck, T., Ceulemans, B., van de Warrenburg, B.P., Zuchner, S., Gonzalez, M.A., Schule, R., Synofzik, M., Van der Aa, N., et al. (2015). First de novo KCND3 mutation causes severe Kv4.3 channel dysfunction leading to early onset cerebellar ataxia, intellectual disability, oral apraxia and epilepsy. BMC Med Genet *16*, 51. 10.1186/s12881-015-0200-3.
82. Gebauer, M., Isbrandt, D., Sauter, K., Callsen, B., Nolting, A., Pongs, O., and Bahring, R. (2004). N-type inactivation features of Kv4.2 channel gating. Biophys J *86*, 210-223. 10.1016/S0006-3495(04)74097-7.
83. Ferrer, T., Cordero-Morales, J.F., Arias, M., Ficker, E., Medovoy, D., Perozo, E., and Tristani-Firouzi, M. (2011). Molecular coupling in the human ether-a-go-go-related gene-

853 1 (hERG1) K+ channel inactivation pathway. J Biol Chem *286*, 39091-39099.
854 10.1074/jbc.M111.292060.

855

Figure legends

Figure 1. Photographs of some of the affected individuals.

Left) Individual 1 throughout the years. Photos and x-rays of her hands and feet, illustrating nail hypoplasia and aplasia, and terminal phalanx hypoplasia (brachytelephalangia). Right) Individual 4, illustrating synophrys and nail hypoplasia.

Figure 2. ***Schematic representation of mutations in Kv2.2 protein.*** **A.** Topology of Kv2.2 channel and schematic representation of distribution of *KCNB2* point mutations. The mutations are in the following regions: c.281G>A, (p.Gly94Glu), c.472A>G, (p.Thr158A)la: N-terminus, c.641C>T, (p.Thr214Met): S1-S2 linker, c.724G>A, (p.Ala242Thr): S2, c.827C>T, (p.Pro276Leu): S3, c.911G>A, (p.Arg304Gln): S4, c.994T>G, (p.Tyr332Asp): S4-S5 linker, c.1124C>T, (p.Ala375Val) , c.1141A>G, (p.Thr381Ala): pore helix, c.1937C>T, (p.Ala646Val) – C terminus. **B.** Alignment of the mutated Kv2.2 amino acids across different species. Homology model and mutation distribution of Kv2.2 as a tetramer (Top view, **C**) and as a monomer (**D**) based on the known structure of the Kv1.2/2.1 chimera[40]. The model was generated using alphafold2[41].

Figure 3. ***Activation properties of Kv2.2 variants.*** **A.** Activation currents from oocytes expressing WT-Kv2.2 and variant channels (expressed in the absence (*top*) and presence (*below*), see methods) were evoked by stepping from -90 mV to voltages ranging from -120 to +100 mV in 10 mV increments for 100 ms. This was followed by a voltage step to -20 mV for 100 ms and back to -90 mv for 5 s to allow recovery of the channels to deactivated states (protocol illustrated in the left corner). c.641C>T, (p.Thr214Met) does not evoke anu currents. c.994T>G, (p.Tyr332Asp) show reduced currents. c.1141A>G, (p.Thr381Ala) shows transient channel opening followed by a rapid inactivation of ionic currents. **B.** Current-voltage (IV) relationship of Kv2.2 variants (*left*) and corresponding box plots of maximal current amplitudes measured at +100 mV (*right*). p.Thr214Met, p.Tyr332Asp and p.Thr381Ala show significant reduction in current amplitudes as compared to WT. **C.** Conductance-Voltage (GV) relationship of KCNB2 variants when expressed in oocytes alone. IV (**D)** and GV (**E**) relationship of Kv2.2 variants when co-expressed with equal amounts of WT. WT:p.Thr214Met show significant reduction in current amplitudes as compared to WT alone. GV curves were best fitted by a sum of two Boltzmann relations of the form $G/Gmax = Bottom + (Top_1\text{-}Bottom)/(1 + \exp((V_{50(1)}\text{-}X)/k_1)) + (Top_2\text{-}Top_1)/(1 + \exp((V_{50(2)}\text{-}X)/k_2))$. The fitting parameters ($V_{50(1)}$,$V_{50(2)}$, k_1 , k_2) for the GV activation relationships have been compiled in **Table 2**. Values are provided as means $\pm$ S.D. from n > 6 oocytes per conditions from at least 2 independent experiments. Statistical significance was tested by Kruskal Wallis one-way analysis of variance followed by Dunn's post-hoc test comparing amplitudes of the different variants to WT. * $p < 0.05$, ** $p < 0.01$, *** $p < 0.001$.

Figure 4. ***Reversal potential of Kv2.2 variants.*** **A.** For calculating the reversal potentials of the Kv2.2 variants, currents were evoked by stepping from -120 mV to +50 mV for 100 ms followed

by voltages ranging from -120 to +50 mV in 10 mV increments for 100 ms. This was followed by a voltage step to -120 mV for 20 ms and back to the holding potential of -90 mv for 5 s to allow recovery of the channels to deactivated states. The external and internal solutions used in these experiments contained K^+ and either $NMDG^+$ or Na^+ in the concentrations mentioned in the figure. **B.** Representative raw traces of the reversal potential protocol in an oocyte expressing WT-Kv2.2 in $NMDG^+$ and K^+ containing external and internal solutions. The resulting IV curves for this protocol of Kv2.2 variants alone (*left*) or co-injected with WT (*right*) in solutions containing either $NMDG^+$ and K^+ (**C**) or Na^+ and K^+ (**D**) are shown. The variants do not seem to alter the K^+ selectivity of the channel pore (X-intercept data compiled with 95% C.I. in **Table S3**).

Figure 5. ***Inactivation features of currents by KCNB2 variants.*** **A.** Protocol to measure voltage dependent inactivation in Kv2.2 variants. To measure inactivation, *c*urrents from oocytes expressing Kv2.2 variant channels were evoked by stepping from -90 mV to voltages ranging from -120 to +40 mV in 10 mV increments for 20 s. This was followed by a voltage step to +60 mV for 100 ms and back to -120 mv for 5 s to allow recovery of the channels from inactivation. The raw traces from voltage steps highlighted in thickened line (-90 mV → 40 mV → 60 mV → 120 mV) are highlighted in **(B)** from oocytes expressing the individual variants alone or in from oocytes expressing both WT and a specific variant **(C)**. c.641C>T, (p.Thr214Met) was excluded in B because of lack of any currents evoked by this variant. Currents evoked by c.1141A>G, (p.Thr381Ala) is represented and further explained below. The inactivation current-voltage (IV) relationship of these recordings are plotted in (**D**) and (**E**), respectively. The IV relationship was best fitted by a sum of two Boltzmann relations of the form $I/Imax = Top + (Bottom_1 - Top)/(1 + \exp((V_{50(1)} - X)/k_1)) + (Bottom_2 - Bottom_1)/(1 + \exp((V_{50(2)} - X)/k_2))$. The fitting parameters ($V_{50(1)}$,$V_{50(2)}$, k_1 , k_2) for the IV relationships have been compiled in **Table 3**. **F.** The fitting function mentioned above also calculates the parameter "$Bottom_2$", which describes the extent of inactivation in these variants expressed either alone (top) or with WT (below). The differences in extent of inactivation between the variants and WT (red dashed lines) were tested for significance using the Kruskal Wallis one-way analysis of variance followed by Dunn's post-hoc test comparing amplitudes of the different variants to WT-KCNB2. * $P \leq 0.05$, ** $P \leq 0.01$,*** $P \leq 0.001$. Values are provided as means $\pm$ S.D. from $n > 6$ oocytes per conditions from at least 2 independent experiments. **G.** Representative current trace of an oocyte expressing only the p.Thr381Ala variant (blue trace) or only WT (black trace). p.Thr381Ala expressing oocytes show diminished currents (blue trace) in the inactivation protocol as compared to WT, in a manner like the activation protocol in Fig. 2 and Fig. 3. H represents the raw traces of the inactivation protocol of residual currents of the p.Thr381Ala variant. **I.** The IV relationship of the p.Thr381Ala mutation (blue line) shows recovery of inactivation with increasing voltages as opposed to WT (dashed fit representing the fit to WT IV shown in **D** and **E**).

Figure 1

Indiv. 1






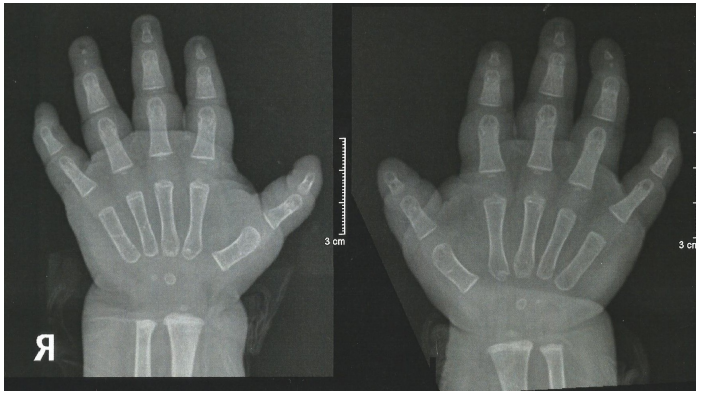

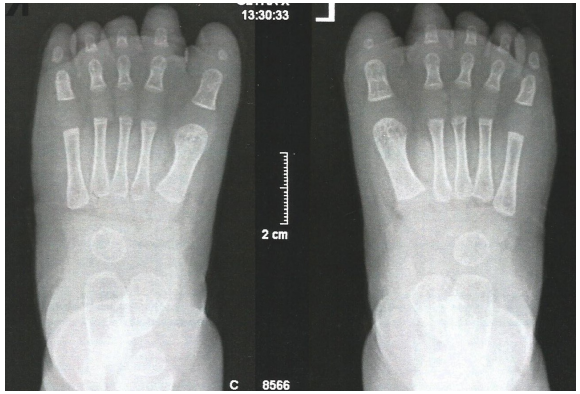

Indiv. 4


Figure 2

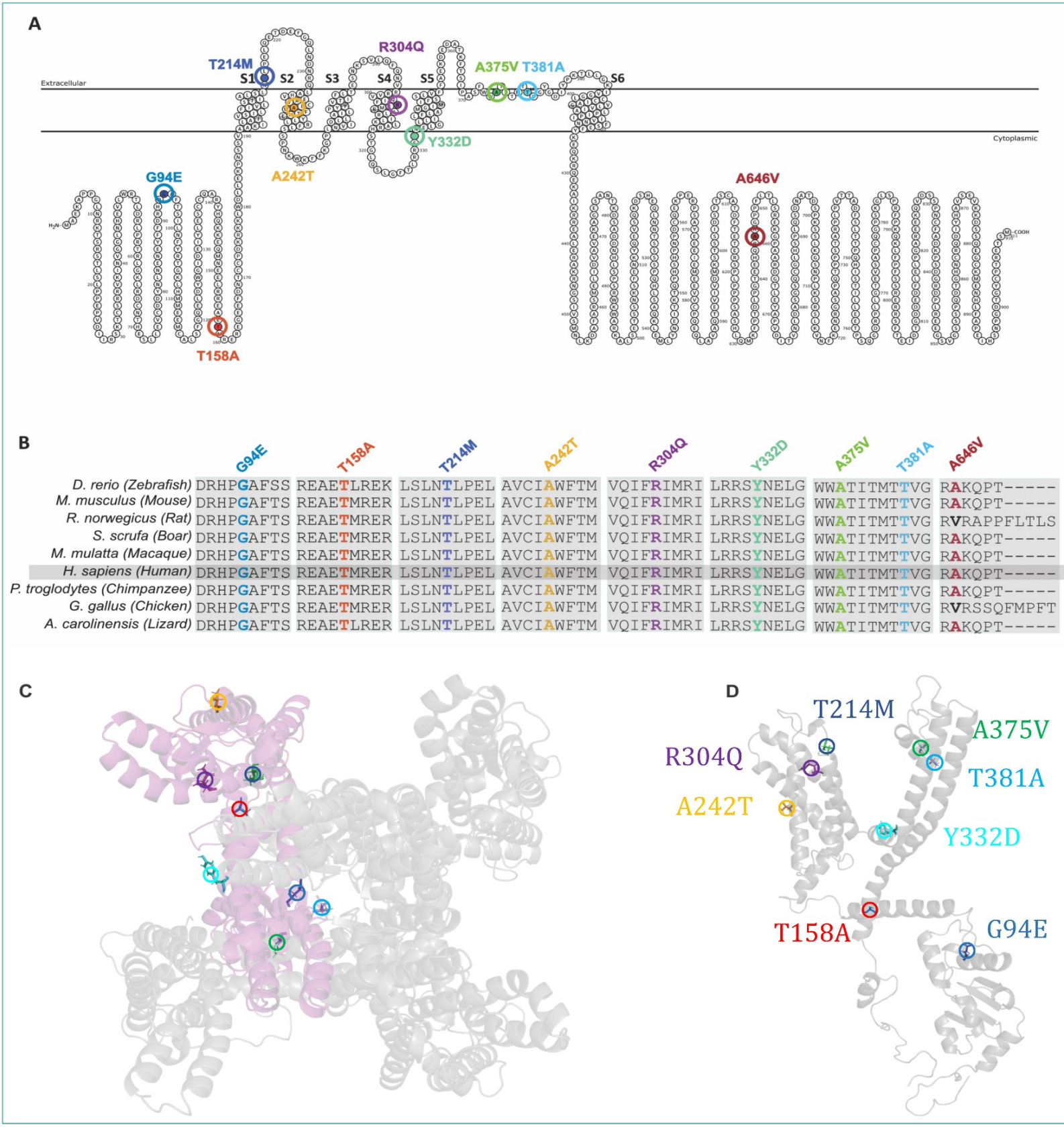
A
Extracellular
Cytoplasmic
S1
S2
S3
S4
S5
S6
T214M
R304Q
A375V
T381A
Y332D
A242T
G94E
A646V
T158A
B
G94E
T158A
T214M
A242T
R304Q
Y332D
A375V
T381A
A646V
D. rerio (Zebrafish) DRHPGAFSS REAETLREK LSLNTLPEL AVCIAWFTM VQIFRIMRI LRRSYNELG WWATITMTTVG RAKQPT-----
M. musculus (Mouse) DRHPGAFTS REAETMRER LSLNTLPEL AVCIAWFTM VQIFRIMRI LRRSYNELG WWATITMTTVG RAKQPT-----
R. norwegicus (Rat) DRHPGAFTS REAETMRER LSLNTLPEL AVCIAWFTM VQIFRIMRI LRRSYNELG WWATITMTTVG RVRAPPFLTLS
S. scrufa (Boar) DRHPGAFTS REAETMRER LSLNTLPEL AVCIAWFTM VQIFRIMRI LRRSYNELG WWATITMTTVG RAKQPT-----
M. mulatta (Macaque) DRHPGAFTS REAETMRER LSLNTLPEL AVCIAWFTM VQIFRIMRI LRRSYNELG WWATITMTTVG RAKQPT-----
H. sapiens (Human) DRHPGAFTS REAETMRER LSLNTLPEL AVCIAWFTM VQIFRIMRI LRRSYNELG WWATITMTTVG RAKQPT-----
P. troglodytes (Chimpanzee) DRHPGAFTS REAETMRER LSLNTLPEL AVCIAWFTM VQIFRIMRI LRRSYNELG WWATITMTTVG RAKQPT-----
G. gallus (Chicken) DRHPGAFTS REAETMRER LSLNTLPEL AVCIAWFTM VQIFRIMRI LRRSYNELG WWATITMTTVG RVRSSQFMPFT
A. carolinensis (Lizard) DRHPGAFTS REAETLRER LSLNTLPEL AVCIAWFTM VQIFRIMRI LRRSYNELG WWATITMTTVG RAKQPT-----
C
D
T214M
A375V
R304Q
T381A
A242T
Y332D
T158A
G94E

Figure 3

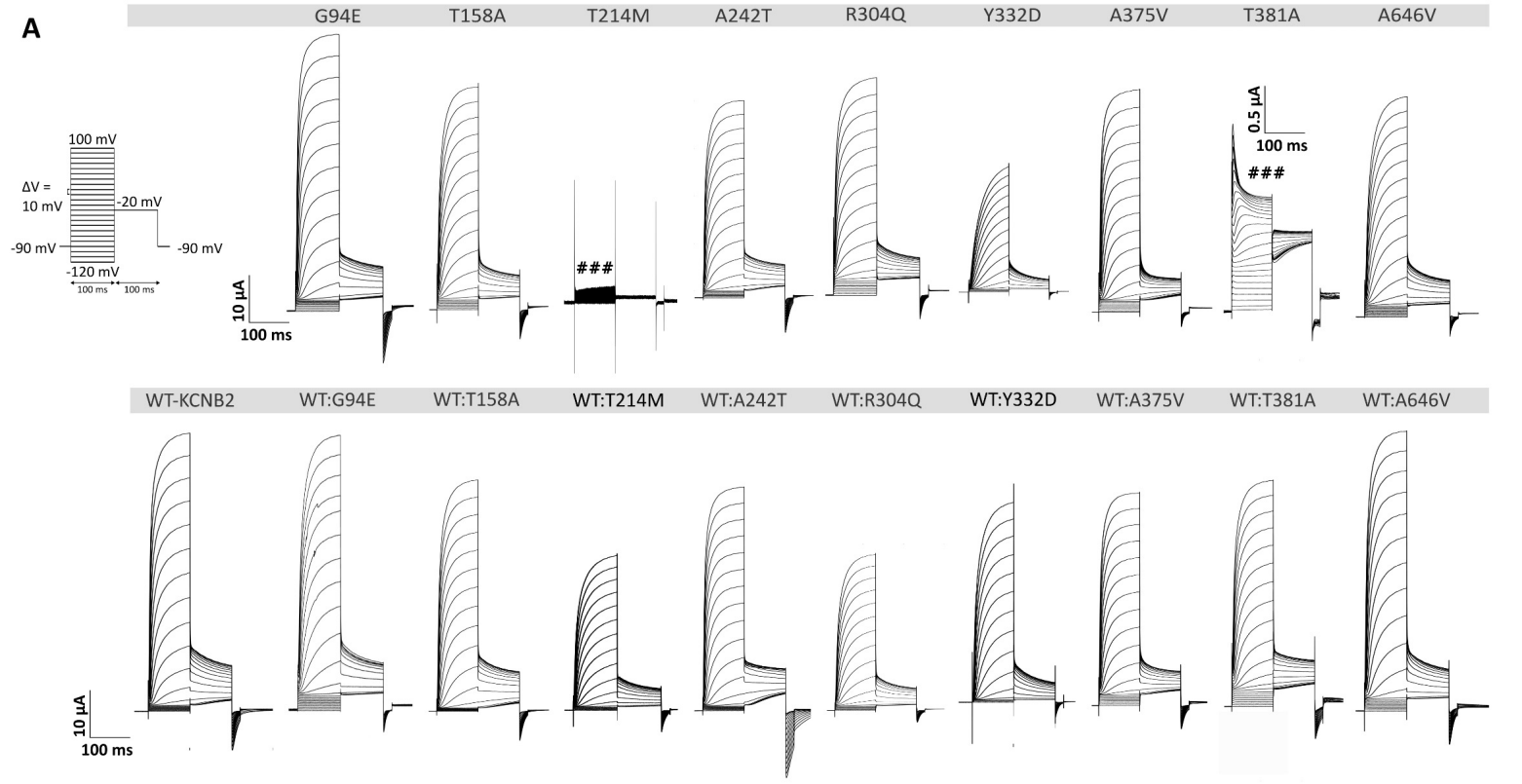
A
G94E
T158A
T214M
A242T
R304Q
Y332D
A375V
T381A
A646V
100 mV
ΔV = 10 mV
-20 mV
-90 mV
-90 mV
-120 mV
100 ms
100 ms
10 µA
100 ms
###
0.5 µA
100 ms
###
WT-KCNB2
WT:G94E
WT:T158A
WT:T214M
WT:A242T
WT:R304Q
WT:Y332D
WT:A375V
WT:T381A
WT:A646V
10 µA
100 ms

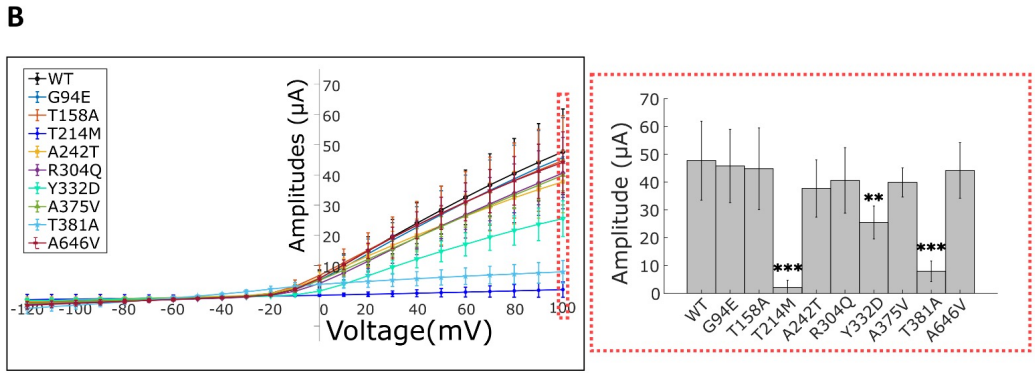
B
WT
G94E
T158A
T214M
A242T
R304Q
Y332D
A375V
T381A
A646V
Amplitudes (µA)
Voltage(mV)
Amplitude (µA)
***
**
***
WT
G94E
T158A
T214M
A242T
R304Q
Y332D
A375V
T381A
A646V

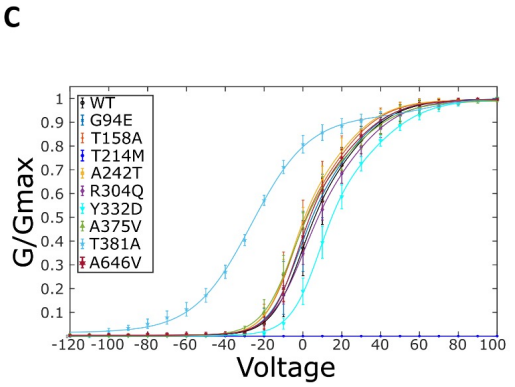
C
WT
G94E
T158A
T214M
A242T
R304Q
Y332D
A375V
T381A
A646V
G/Gmax
Voltage

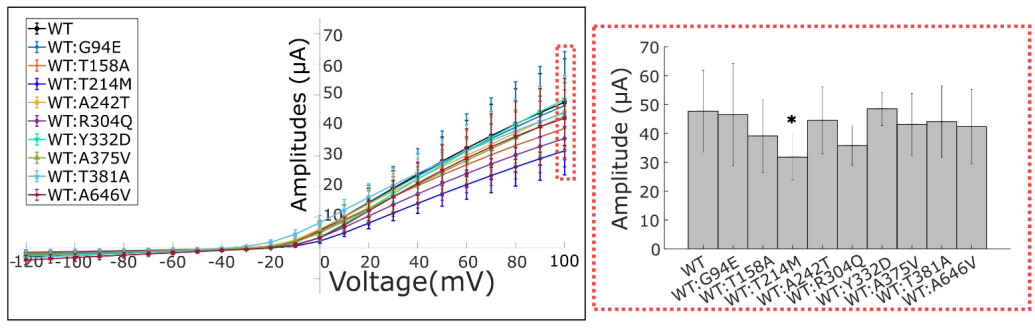
D
WT
WT:G94E
WT:T158A
WT:T214M
WT:A242T
WT:R304Q
WT:Y332D
WT:A375V
WT:T381A
WT:A646V
Amplitudes (µA)
Voltage(mV)
Amplitude (µA)
*
WT
WT:G94E
WT:T158A
WT:T214M
WT:A242T
WT:R304Q
WT:Y332D
WT:A375V
WT:T381A
WT:A646V

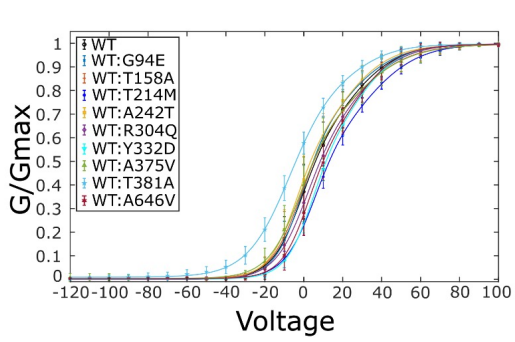
E
WT
WT:G94E
WT:T158A
WT:T214M
WT:A242T
WT:R304Q
WT:Y332D
WT:A375V
WT:T381A
WT:A646V
G/Gmax
Voltage

Figure 4

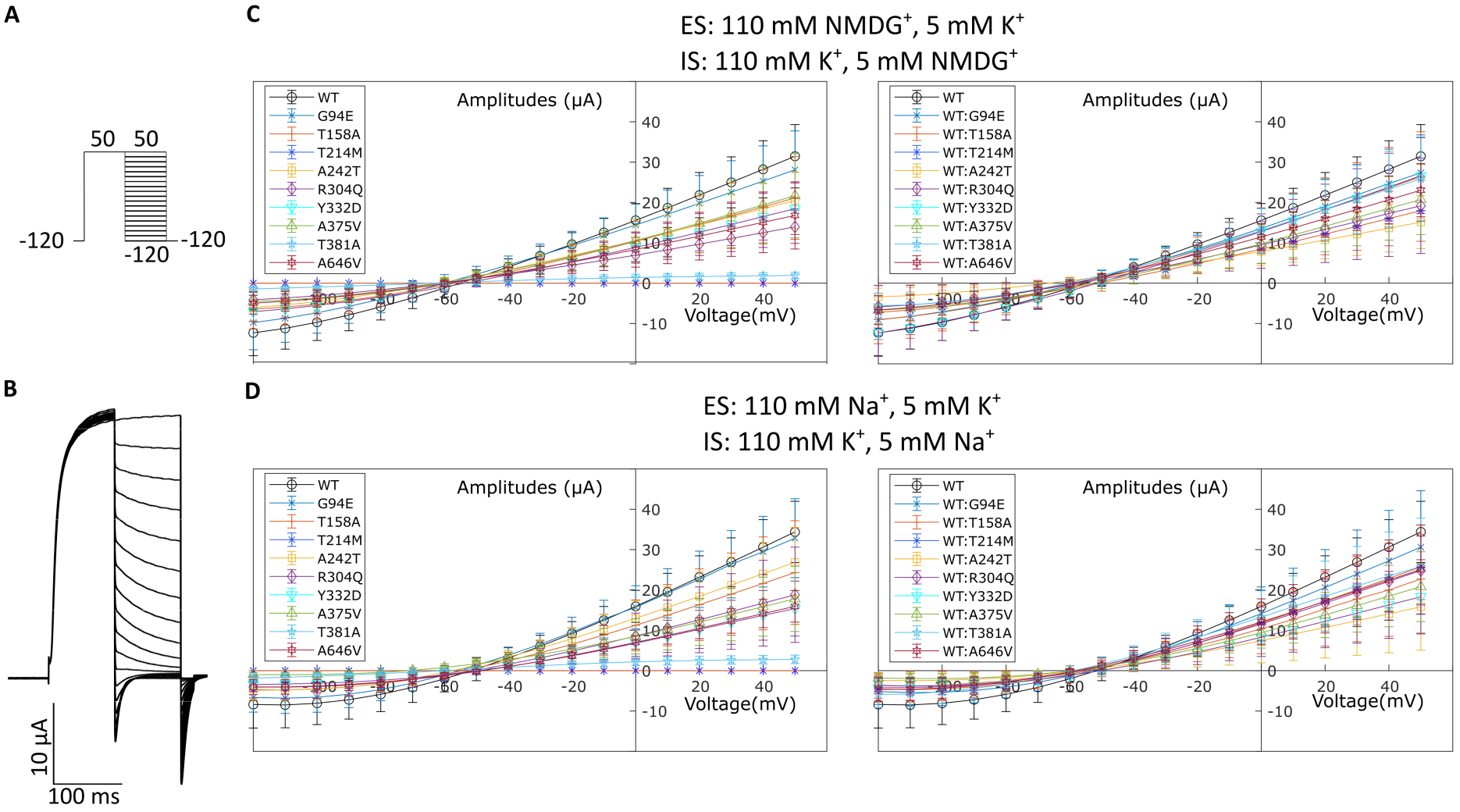
A
50
50
-120
-120
-120
B
10 µA
100 ms
C
ES: 110 mM NMDG+, 5 mM K+
IS: 110 mM K+, 5 mM NMDG+
Amplitudes (µA)
Voltage(mV)
WT
G94E
T158A
T214M
A242T
R304Q
Y332D
A375V
T381A
A646V
WT:G94E
WT:T158A
WT:T214M
WT:A242T
WT:R304Q
WT:Y332D
WT:A375V
WT:T381A
WT:A646V
D
ES: 110 mM Na+, 5 mM K+
IS: 110 mM K+, 5 mM Na+

Figure 5

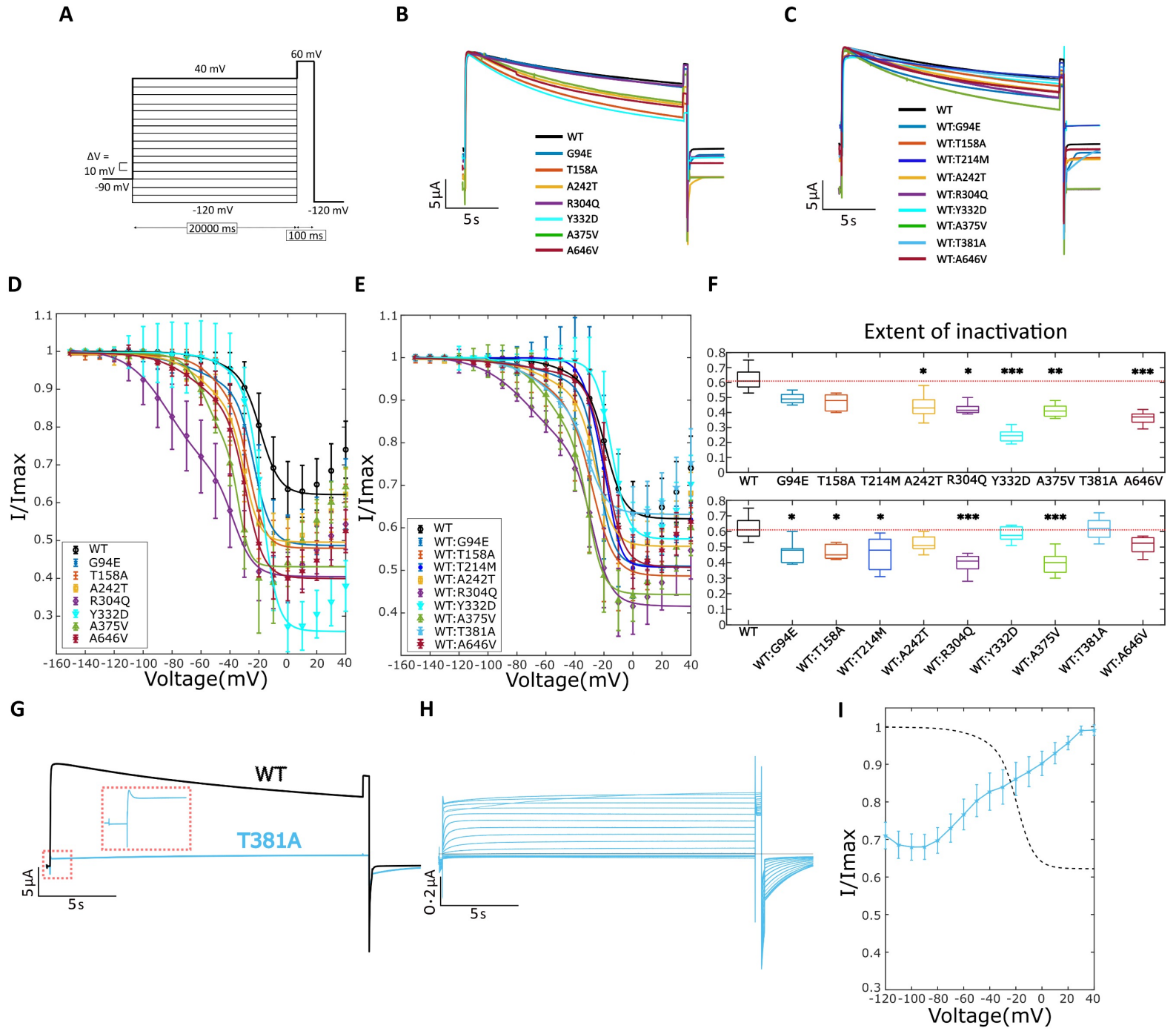
A
60 mV
40 mV
ΔV =
10 mV
-90 mV
-120 mV
-120 mV
20000 ms
100 ms
B
WT
G94E
T158A
A242T
R304Q
Y332D
A375V
A646V
5 µA
5 s
C
WT
WT:G94E
WT:T158A
WT:T214M
WT:A242T
WT:R304Q
WT:Y332D
WT:A375V
WT:T381A
WT:A646V
5 µA
5 s
D
I/Imax
Voltage(mV)
E
I/Imax
Voltage(mV)
F
Extent of inactivation
WT G94E T158A T214M A242T R304Q Y332D A375V T381A A646V
WT WT:G94E WT:T158A WT:T214M WT:A242T WT:R304Q WT:Y332D WT:A375V WT:T381A WT:A646V
G
WT
T381A
5 µA
5 s
H
0.2 µA
5 s
I
I/Imax
Voltage(mV)

Supplemental Note: Case Reports

Proband 1

***KCNB2* variant:** c.1141A>G, p.Thr381Ala, *de novo*

Method of Identification: Trio exome and sanger sequencing

Patient information: The patient exhibited global developmental delay, hypotonia and intellectual disability but no autistic traits. The disease phenotype overlapped partially with Zimmerman-Laband and DOORS syndromes, which are neurodevelopmental disorders with epilepsy and hypoplasia of the terminal phalanges and nails. She also exhibited dysmorphisms that included abnormal nails, mild blepharoptosis, beaked nose, flat midface, open mouth, drooling, full lower lip. She has no family history. She was born at term by C-section. Birth weight was 2.79 kg and length was 48 cm. The patient age at last visit was 5 years with a height of 107.5 cm and a weight of 19.7 kg. She exhibited epileptic seizures with effective treatment with Levetiracetam. Her MRI exhibited prominence of the anterior horn of lateral ventricle and 3rd ventricle and decreased bilateral hippocampus. She exhibited aortic dilation and neurogenic bladder. Other clinical features include diabetes, cataract, gingival fibromatosis, cortical vision impairment, Duane syndrome, hyperopia, astigmatism, low bone density, oropharyngeal dysphagia, cataract, and low bone density.

Proband 2

***KCNB2* variant:** c.281G>A, p.Gly94Glu, *de novo*

Method of Identification: Whole exome and Trio whole genome sequencing

Patient information: The patient, at two years of age, exhibited developmental delay but was making slow progress. He rolled at 6 months, sat at 2 years (propped), and could sit independently (but not stand unsupported) at 2.5 years. He exhibited language delay but made sounds and coos at 2.5 years. At this age, the patient is too young to assess for intellectual disability and autistic traits and no seizures were noted. Neurological assessment revealed Hypotonic/ataxic cerebral palsy per neurology. He also exhibited dysmorphisms that included synophrys and full lashes, single transverse palmar crease on one side, high palate and clinodactyly. The patient had no immediate family history, but there are some still births in extended family (maternal side) and a maternal cousin with possible autism spectrum disorder. The patient was born at 38 5/7 weeks to a G1 P0->1 mother with appropriate prenatal care and no exposures reported. Fetal ultrasound was normal except for concern for small cerebellum. Birth weight was 3.152 kg, length was 50.8 cm, head circumference was 32.3 cm and APGAR score of 7/8. Age at last visit was 2.5 years with weight of 14.8 kg (77th percentile based on CDC boys 2-20 years), height of 98 cm (94th percentile), and head circumference of 48.7 cm (33rd percentile). Other anomalies include bbnormal trabeculation of left ventricular myocardium and slight

shawl scrotum. Other clinical features include delayed visual maturation and bilateral sensorineural hearing loss.

Proband 3

***KCNB2* variant:** c.1937C>T, p.Ala646Val, Inherited

Method of Identification: Trio whole exome and whole genome sequencing

Patient information: The patient exhibited delayed motor milestones, speech and language delay, apraxia, weakness, easily fatigue, irritability, regression, intellectual disability, and other neurodevelopmental disorders but no autistic traits. No seizures were noted. She also exhibited macrocephaly, deep set eyes, broad forehead, horizontal palpebral fissures, thin upper lips, tapered fingers and puffy feet. The patient inherited the mutation from her father in an autosomal dominant manner who was symptomatic with pneumothorax, pain, hypotonia, joint pain, weakness, fatigue and clumsiness. Her brother was also symptomatic who was positive for neurodevelopmental disorder, abnormal EEG, hypotonia, pain, and apraxia. The patient was born at term by C-section. Her birth growth parameters are unavailable. Her age at last visit was 3 years (in 2020) with a head circumference of 52 cm (98% percentile). Other clinical features include microscopic hematuria, episodic edema, and rashes.

Proband 4

***KCNB2* variant:** c.641C>T, p.Thr214Met, *de novo*

Method of Identification: Trio whole exome sequencing

Patient information: The patient was born at term with a weight of 4.24 kg, length of 53 cm and head circumference of 37 cm. He started walking at 17 months and exhibited language delay, intellectual disability, and mild autistic traits in infancy. No seizures were noted. He also exhibited synophrys, nail hypoplasia and myopia. The patient had no family history, and the age of last visit was 18 years. His growth parameters at this stage included a weight of 64 kg, height of 183 cm and head circumference of 59.5 cm.

Proband 5

***KCNB2* variant:** c.994T>G, p.Tyr332Asp, *de novo*

Method of Identification: Trio whole exome sequencing

Patient information: The patient exhibited severe global developmental delay and intellectual disabilty. According to BSID-III, she exhibited motor development p1.8, cognitive development index of 64% (cognitive age of 9 months at age 15.7 months) and language index of 72%. She couldn’t walk independently yet with no speech and proximal hypertonia. Slow progress was observed with no regression. . Patient exhibited dysmorphisms in the hands and in the head. The latter included frontal bossing, suggestion of macrocephaly (but not on measurement) and broad forehead. She was born at term by C-section and had normal birth weight (3.335 kg). Her age at last visit

was 21 months with head circumference of 49.5 cm (+1SD). She has a family history of hypertension and obesity. Brain anomalies include delayed myelination, T2 abnormalities in basal ganglia (hyperintensity in globus pallida or hypo-intensity of other ganglia), small volume of thalamus, subtle increased volume of lateral and 3rd ventricles and peripheral CSF, small corpus callosum (especially the posterior part), subtle small volume of adenohypophysis, small cerebellar hemisphere on the left side and cyst in the left temporal side. Other neurological features include tongue protrusion, severe strabismus and retinal 'bear tracks'.

Proband 6

***KCNB2* variant:** c.911G>A, p.Arg304Gln, *de novo*

Method of Identification: Trio whole exome sequencing

Patient information: The patient exhibited delayed motor milestones, speech and language delay with intellectual disability and autistic traits. Other neurological features include ADHD, mood disorder and aggressive behavior. Facial dysmorphisms include double hair whorl, malar flattening, long philtrum, up-slanting palpebral fissures, epicanthal folds and broad nasal tip. He also had tapered fingers and short toes. He was born at term by vaginal delivery and had a birth weight of 3.28 kg. His age and height at last visit were 9 years and 135.9 cm, respectively. Family history included mental health issues in paternal uncle and paternal grandmother.

Proband 7

***KCNB2* variant:** c.827C>T, p.Pro276Leu, mosaic in proband (47T, 72C)

Method of Identification: Trio whole exome sequencing

Patient information: The patient exhibited normal motor development with language delay and moderate intellectual disability. He had behavioural issues that were treated with Risperidone, Fluoxetine, Guanfacine and methylphenidate. He suffers from drug-resistant focal and generalized seizures (Age of onset: 3 years and 9 months) that show multifocal abnormalities with frontal predominance on EEG. Previous anti-seizure medications (ASM) include Ethosuximide, VPA, perampanel, topiramate, clobazam, rufinamide, memantine, levetiracetam, IVIG; Current ASM include Lamotrigine, Oxcarbazepine, Sulthiame, Vagal Nerve Stimulator and Diazepam *prn*. Other neurological features include diadochokiensia with monopedal stand more insecure on the left. No brain abnormalities were detected except for non-specific prominent perivascular spaces. He was born at term, Apgar score of 2-6-9 with no perinatal complications. His age at last visit was 15 years with the head circumference of 51.7 cm, height of 150.6 cm and weight at 52 kg. Family history was unremarkable; the father was mosaic with sequencing reads for both T and C nucleotides (17T, 192C).

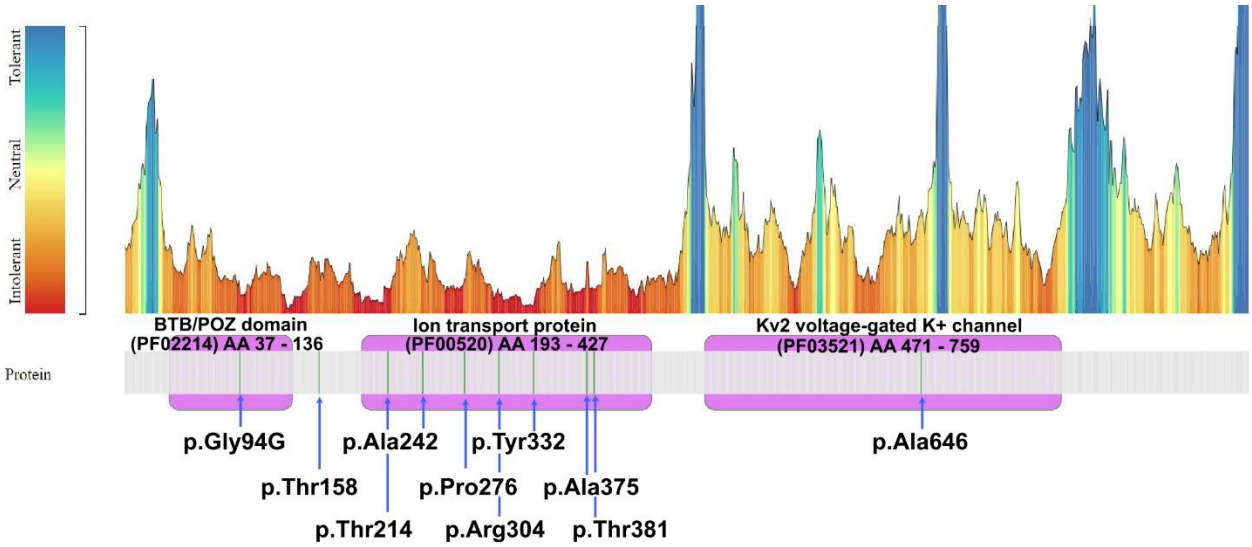

Figure S1. Metadome's missense tolerance landscape for KCNB2 (NM_004770.2). All amino acids are intolerant to missense variants (scores in Table S2).

Table S1. Primers used for mutagenesis.

KCNB2 (NM_004770.3) variants	Forward primer	Reverse primer
c.281G>A, p.Gly94Glu	aaatggaagtgaaggcttctggatgccgatcaaag	ctttgatcggcatccagaagccttcacttccattt
c.472A>G, p.Thr158Ala	cgctctcgcatagcctctgcctctcgc	gcgagaggcagaggctatgcgagagcg
c.641C>T, p.Thr214Met	ccattgctttgtctctcaatatgctgccggagc	gctccggcagcatattgagagacaaagcaatgg
c.724G>A, p.Ala242Thr	tccatggtaaaccatgtaatacacacagcctccac	gtggaggctgtgtgtattacatggtttaccatgga
c.911G>A, p.Arg304Gln	gaggatgcgcatgatttggaagatctggaccac	gtggtccagatcttccaaatcatgcgcatcctc
c994T>G, p.Tyr332Asp	tttcacccttaggcggagtgacaatgaattgggct	agcccaattcattgtcactccgcctaagggtgaaa
c.1141A>G, p.Thr381Ala	tcaccatagccaacagcggtcatggtgatggtg	caccatcaccatgaccgctgttggctatggtga
c.1124C>T, p.Ala375Val	ggtcatggtgatggtgacccaccaaaatgatgc	gcatcattttggtgggtcaccatcaccatgacc
c.1937C>T, p.Ala646Val	ggggggcccctaactctttggtgctcttct	agaagagcaccaaagagttaggggcccccc

Table S2. Summary of *in-silico* predictions for all *KCNB2* variants reported in our study

ACMG classification of variants (not taking into account functional data presented here), metadome amino acid missense tolerance scores and pathogenicity prediction and conservation scores obtained using Ensembl's VEP NB. Definition of acronyms and details on the scores with links and references for the tools can be found in the dbNSFP v4 "read me" file at https://usf.app.box.com/s/6yi6huheisol3bhmld8bitcon1oi53pm

See excel file for data.

Table S3. Reversal potential of Kv2.2 variants

Variants	Without WT	With WT	Without WT	With WT
	ES: 110 $NMDG^+$, 5 K^+; IS: 110 K^+, 5 $NMDG^+$		ES: 110 Na^+, 5 K^+; IS: 110 K^+, 5 Na^+	
	V_{rev} in mV (95% C.I.)			
WT	-60.8 (-59.2 to -62.6)		-63.8 (-61.7 to -65.9)	
G94E	-65.3 (-60.8 to -70.1)	-64.3 (-61.1 to -67.6)	-67.6 (-62.8 to -72.8)	-68.1 (-62.1 to -74.8)
T158A	-64.8 (-59.1 to -71.2)	-62.9 (-58.3 to -68.0)	-67.4 (-61.5 to -74.1)	-70.0 (-61.3 to -80.5)
T214M	n.a.	-58.0 (-52.9 to -63.5)	n.a.	-68.3 (-63.6 to -73.4)
A242T	-68.0 (-63.6 to -72.8)	-72.9 (-66.7 to -79.9)	-70.1 (-65.7 to -75.0)	-70.7 (-62.0 to -81.1)
R304Q	-67.6 (-63.5 to -72.0)	-65.0 (-58.6 to -72.1)	-65.0 (-58.0 to -73.0)	-70.7 (-65.5 to -76.4)
Y332D	-60.4 (-56.6 to -64.4)	-56.6 (-53.4 to -60.0)	-64.2 (-58.2 to -70.9)	-64.0 (-57.9 to -70.7)
A375V	-71.2 (-64.9 to -78.3)	-62.0 (-57.6 to -66.7)	-81.6 (-75.5 to -88.6)	-75.2 (-68.9 to -82.4)
T381A	-60.0 (-54.0 to -66.7)	-70.4 (-65.3 to -75.9)	-60.7 (-55.9 to -66.0)	-68.8 (-63.3 to -75.0)
A646V	-66.5 (-60.9 to -72.6)	-66.7 (-62.9 to -70.8)	-61.8 (-57.8 to -66.0)	-69.9 (-64.0 to -76.5)

n.a. - not analysed; the amplitudes were too low for determination of reversal potential.

C.I. - Confidence Intervals